JOURNAL OF SPACECRAFT AND ROCKETS
Vol. 56, No. 5, September–October 2019

Relative Motion Dynamics in the Restricted Three-Body Problem

Giovanni Franzini* and Mario Innocenti†
University of Pisa, 56122 Pisa, Italy

DOI: 10.2514/1.A34390

This paper discusses the derivation and simplification of equation sets for the relative motion dynamics characterization in the restricted three-body problem. As opposed to previous models proposed in the literature, the relative motion is studied in a frame local to the target spacecraft, the local-vertical local-horizon frame, and spacecraft state is expressed with respect to the primary about which they are orbiting. The exact description of the relative dynamics is derived, as well as simplified equation sets based on both the elliptic and the circular restricted three-body problems. The accuracy of the simplified sets is analyzed by means of extensive numerical simulations on a realistic rendezvous scenario with a target on lunar orbit.

Nomenclature

G	=	universal gravitational constant
M_i	=	primary body i mass
m_i	=	spacecraft i mass
$\boldsymbol{R}_i$	=	inertial position of i
$\boldsymbol{r}_{ij}$	=	position of i with respect to j
$\boldsymbol{h}_{i/j}$	=	angular momentum of i with respect to j
$\mathcal{I}$: $\{O; \hat{\boldsymbol{I}}, \hat{\boldsymbol{J}}, \hat{\boldsymbol{K}}\}$	=	inertial frame centered in O
$\mathcal{M}$: $\{\boldsymbol{R}_m; \hat{\boldsymbol{\imath}}_m, \hat{\boldsymbol{\jmath}}_m, \hat{\boldsymbol{k}}_m\}$	=	Moon (synodic) frame centered on the Moon inertial position $\boldsymbol{R}_m$
$\mathcal{L}$: $\{\boldsymbol{R}_t; \hat{\boldsymbol{\imath}}, \hat{\boldsymbol{\jmath}}, \hat{\boldsymbol{k}}\}$	=	local-vertical local-horizon frame centered on the target center of mass $\boldsymbol{R}_t$
$\mu_i = GM_i$	=	gravitational parameter of the primary body i
$\boldsymbol{\rho}$	=	chaser position with respect to the target
$\boldsymbol{\omega}_{i/j}$	=	angular velocity of i with respect to j
$[\dot{\boldsymbol{v}}]_{\mathcal{F}}$	=	time derivative of vector $\boldsymbol{v}$ in the frame $\mathcal{F}$

I. Introduction

THE study of the spacecraft relative dynamics is one of the most trending topics in the space research field. As a matter of fact, the characterization of the relative motion is a critical step in the design and the analysis of all the space missions requiring the coordination of two or more spacecraft. Notable examples are rendezvous and docking missions and formation flying, which have drawn the interest of the space community for decades. Worth of mention are also future missions such as in-orbit servicing, debris mitigation, and assembly of large orbital structures, which are increasing the interest in the subject.

Relative motion in the two-body problem and, in particular, in near-Earth orbits has been studied extensively. The first and most remarkable models were proposed during the 1960s: the *Clohessy–Wiltshire equations* [1] and the *Tschauner–Hempel equations* [2]. For years, these sets of equations have been the model of reference for the analysis and the design of relative guidance, navigation, and control systems [3], because they provide linear models for the study of relative motion in circular and elliptic orbits. However, the two sets are based on the following main assumptions: the spacecraft relative separation is significantly small compared with the distance from the primary body center of mass, and no orbital perturbations act on them. These assumptions limit the use of the two equation sets in applications such as formation flying, which generally requires to maintain formations over long mission times, while satisfying high-accuracy requirements in order to meet the mission objectives [4]. In such cases orbital perturbation must be taken into account in order to predict the long-term motion, and the linearization error may be non-negligible if long baselines are considered. Therefore, a wide variety of models have been proposed in the literature to overcome these limitations [5].

The attention received by the study of relative motion in three-body scenarios is not comparable to the two-body case. Depending on the three-body system considered, when the spacecraft fly near the biggest primary, the influence of the second primary is generally modeled as an orbital perturbation (*third-body perturbation*), as in [6–8]. However, several missions under study are targeting celestial bodies where the third-body influence must be explicitly taken into account in the relative dynamics. Two examples are *Phobos Sample Return* mission [9] and the *Human Lunar Exploration Precursor Program* (HLEPP) [10,11]. With reference to the former, the orbital dynamics around Phobos is particularly complex, because the small mass-ratio and length-scale of the Mars–Phobos system result in a sphere of influence of the Martian moon, which is very close to its surface. Hence, the two-body problem is an inaccurate approximation of the spacecraft's dynamics in the vicinity of Phobos [12]. In the HLEPP an habitable station, the *Deep Space Gateway* (DSG), will fly a *near-rectilinear halo orbit* (NRHO). Again, two-body-based equation sets cannot be used in this context, because non-Keplerian orbits typical of three-body systems are considered, and models based on the two-body problem generally exploit the characteristic of the Keplerian orbits. Therefore, ad hoc models for relative motion description in the three-body problem must be identified.

The approach generally adopted in the literature is based on the numerical computation of the difference between the equations that regulate the motion of the two spacecraft. More specifically, the *circular restricted three-body problem* (CR3BP) is used to model the single spacecraft dynamics, and then the difference is used to numerically describe the relative motion. Examples of this kind of approach applied to formation-flying and rendezvous missions can be found in [13–15]. This type of description has two main limitations. First the use of CR3BP equations is inaccurate for some three-body systems, as, for instance, in the Earth–Moon and in the Mars–Phobos cases, where the system eccentricity has a non-negligible influence; see [16] and [12], respectively. Hence, the *elliptic restricted three-body problem* (ER3BP) must be considered. Second, these sets are developed in a frame rotating with the primaries, generally referred to as the *synodic* or *pulsating reference frame*, and centered on one of them, or on their common center of mass, or even in a libration point. Historically, relative motion, especially in rendezvous missions, is studied in a frame local to the *target* or *leader* spacecraft, such as the *local-vertical local-horizon*

Received 10 September 2018; revision received 30 January 2019; accepted for publication 12 March 2019; published online 22 April 2019.

*Department of Information Engineering; currently Senior Research Scientist, United Technologies Research Centre Ireland, 2nd Floor, Penrose Wharf, Penrose Business Centre, Cork T23 XN53, Ireland; franzigi@utrc.utc.com (Corresponding Author).

†Full Professor, Department of Information Engineering, Largo L. Lazzarino 1; mario.innocenti@unipi.it. Associate Fellow AIAA.

(LVLH) frame. This choice eases the integration of measurements acquired by spacecraft relative positioning sensors. In addition, the use of a local frame allows to better understand and to characterize the *chaser* or *follower* dynamics as seen from the target/leader. This is particularly important in rendezvous and docking missions, in order to analyze and to assess the safety of the maneuvers performed by an incoming chaser spacecraft [3]. Some studies try to solve these limitations. For instance, local frames are considered in [17–19], but only for the analysis and the visualization of the results, not for derivation of the equations of relative motion. The general restricted three-body problem setup is considered in [20], but spacecraft position and velocity is considered with respect to the Sun-Earth L2 libration point, and the relative motion is expressed in the synodic frame.

In this paper we propose a characterization of the relative dynamics in a restricted three-body context as seen in a frame local to a target. In particular, we consider a pair of spacecraft, in the following referred to as chaser and target, flying in the vicinity of the smallest primary, in a region where the third-body effect must be explicitly considered into the relative dynamics. Spacecraft position and velocity vectors are expressed with respect to the smallest primary center of mass. Considering, for instance, the Earth–Moon system, this feature is particularly useful in the case one of the spacecraft loses the line of sight with the ground stations on Earth, because measurements are taken with respect to the Moon. In addition, target orbits in restricted three-body scenarios are generally expressed with respect to the smallest primary. The LVLH frame centered on the target is used as a local frame. As opposed to [17–19], the LVLH frame is defined with reference to the smallest primary, in analogy with the frame definition used for rendezvous in Earth orbits, because vehicles incoming from its surface are expected to approach the target. A general set of equations of relative motion in the restricted three-body problem is derived. Conversely to the aforementioned references, the derivation is performed directly in the LVLH frame, making the resulting equation set particularly appealing for rendezvous and docking operations. The only assumption made is the spacecraft having negligible masses with respect to the primaries. Thus, the equations have general validity, and are not restricted to the elliptic or circular three-body problem. Then, the ER3BP and the CR3BP are considered, in order to derive simplified equation sets. A linearization of the sets is also performed in order to provide linear models useful for preliminary relative guidance, navigation, and control system design. The accuracy of the equation sets is analyzed by means of extensive Monte Carlo simulations. The HLEPP is used as a reference mission scenario, and an Earth–Moon NRHO is considered for the target. Linear two-body-based equation sets were also considered in the analysis, and their accuracy compared against the three-body based sets. Given the chosen reference mission, and in order to ease the general readability, in the paper we will refer to the Earth–Moon system. Nevertheless, application of the proposed equation to other three-body systems is straightforward, because the simplifications considered in the paper are not based on any peculiar characteristic of the lunar orbit or of the Earth–Moon system.

The paper is organized as follows. In Sec. II a brief review of the ER3BP and of the CR3BP is provided, and the spacecraft equations of motion with respect to the Moon are derived. Section III discusses the derivation of equations of relative motion for the exact description of the relative dynamics of a chaser spacecraft with respect to a target in the restricted three-body problem context. Possible simplifications of the relative dynamics are discussed in Sec. IV, where four equation sets are derived. The accuracy of the sets is analyzed in Sec. V. Conclusions are drawn in Sec. VI.

II. Restricted Three-Body Dynamics

Consider the three-body system composed by the Earth and the Moon *primary bodies* and a spacecraft i, with masses M_e, M_m, and m_i, respectively. Their positions with respect to an *inertial frame* $\mathcal{I}$ is denoted with $\boldsymbol{R}_e$, $\boldsymbol{R}_m$, and $\boldsymbol{R}_i$, respectively.

Each body exerts its gravitational influence on the others, resulting in the following equations of motion for the three bodies:

$$m_i[\ddot{\boldsymbol{R}}_i]_{\mathcal{I}} = -G\frac{M_e m_i}{r_{ei}^3}\boldsymbol{r}_{ei} - G\frac{M_m m_i}{r_{mi}^3}\boldsymbol{r}_{mi}$$

$$M_e[\ddot{\boldsymbol{R}}_e]_{\mathcal{I}} = G\frac{M_m M_e}{r_{em}^3}\boldsymbol{r}_{em} + G\frac{m_i M_e}{r_{ei}^3}\boldsymbol{r}_{ei}$$

$$M_m[\ddot{\boldsymbol{R}}_m]_{\mathcal{I}} = -G\frac{M_e M_m}{r_{em}^3}\boldsymbol{r}_{em} + G\frac{m_i M_m}{r_{mi}^3}\boldsymbol{r}_{mi}$$

where $\boldsymbol{r}_{ei} = \boldsymbol{R}_i - \boldsymbol{R}_e$ and $\boldsymbol{r}_{mi} = \boldsymbol{R}_i - \boldsymbol{R}_m$ denote the position of the spacecraft i with respect to the Earth and to the Moon, $\boldsymbol{r}_{em} = \boldsymbol{R}_m - \boldsymbol{R}_e$ is the position of the Moon with respect to the Earth, and G is the *universal gravitational constant*. Relative positions norms are indicated with r_{ei}, r_{mi}, and r_{em}. The notation $[\ddot{\boldsymbol{R}}]_{\mathcal{I}}$ denotes the acceleration of the body as seen from the inertial frame.

Equations of motion of spacecraft i with respect to the Earth and to the Moon are then given by:

$$[\ddot{\boldsymbol{r}}_{ei}]_{\mathcal{I}} = [\ddot{\boldsymbol{R}}_i]_{\mathcal{I}} - [\ddot{\boldsymbol{R}}_e]_{\mathcal{I}} = -G\frac{(M_e + m_i)}{r_{ei}^3}\boldsymbol{r}_{ei} - GM_m\left(\frac{\boldsymbol{r}_{mi}}{r_{mi}^3} + \frac{\boldsymbol{r}_{em}}{r_{em}^3}\right) \tag{1}$$

$$[\ddot{\boldsymbol{r}}_{mi}]_{\mathcal{I}} = [\ddot{\boldsymbol{R}}_i]_{\mathcal{I}} - [\ddot{\boldsymbol{R}}_m]_{\mathcal{I}} = -G\frac{(M_m + m_i)}{r_{mi}^3}\boldsymbol{r}_{mi} - GM_e\left(\frac{\boldsymbol{r}_{ei}}{r_{ei}^3} - \frac{\boldsymbol{r}_{em}}{r_{em}^3}\right) \tag{2}$$

We now assume that the mass of the spacecraft i is negligible with respect to the primaries masses (i.e., $m_i \ll M_e$ and $m_i \ll M_m$); that is, we consider the *restricted three-body problem*. Under this assumption the orbital motion of the two primaries is not affected by the spacecraft, and Eqs. (1) and (2) simplify to:

$$\begin{aligned}[\ddot{\boldsymbol{r}}_{ei}]_{\mathcal{I}} &= -\mu_e\frac{\boldsymbol{r}_{ei}}{r_{ei}^3} - \mu_m\left(\frac{\boldsymbol{r}_{mi}}{r_{mi}^3} + \frac{\boldsymbol{r}_{em}}{r_{em}^3}\right)\\ [\ddot{\boldsymbol{r}}_{mi}]_{\mathcal{I}} &= -\mu_m\frac{\boldsymbol{r}_{mi}}{r_{mi}^3} - \mu_e\left(\frac{\boldsymbol{r}_{ei}}{r_{ei}^3} - \frac{\boldsymbol{r}_{em}}{r_{em}^3}\right)\end{aligned} \tag{3}$$

where $\mu_e = GM_e$ and $\mu_m = GM_m$ are the primaries' *gravitational parameters*.

Assume now that the primaries revolve around their common barycenter in elliptic orbits (*elliptic restricted three-body problem*). The motion of the two primaries can then be obtained from the solution of the classical two-body problem.

The equations of motion for the spacecraft i are generally written in a frame that rotates with the primaries. A *Moon* or *synodic reference frame* $\mathcal{M}$: $\{\boldsymbol{R}_m; \hat{\boldsymbol{\imath}}_m, \hat{\boldsymbol{\jmath}}_m, \hat{\boldsymbol{k}}_m\}$ is introduced, with origin in the Moon center of mass, and unit vectors defined as follows:

$$\hat{\boldsymbol{\imath}}_m = -\frac{\boldsymbol{r}_{em}}{r_{em}}, \qquad \hat{\boldsymbol{\jmath}}_m = \hat{\boldsymbol{k}}_m \times \hat{\boldsymbol{\imath}}_m, \qquad \hat{\boldsymbol{k}}_m = \frac{\boldsymbol{h}_{m/e}}{h_{m/e}},$$

where $\boldsymbol{h}_{m/e} = \boldsymbol{r}_{em} \times [\dot{\boldsymbol{r}}_{em}]_{\mathcal{I}}$ is the *specific angular momentum* of the Moon with respect to the Earth, and $h_{m/e} = \|\boldsymbol{h}_{m/e}\|$; see Fig. 1. The Earth–Moon system, and consequently the frame $\mathcal{M}$, rotates with respect to the inertial frame $\mathcal{I}$ with angular velocity $\boldsymbol{\omega}_{m/i} = \omega_{m/i}\hat{\boldsymbol{k}}_m$.

The acceleration of the spacecraft i in the frame $\mathcal{M}$ is given by:

$$\begin{aligned}[\ddot{\boldsymbol{r}}_{mi}]_{\mathcal{I}} = [\ddot{\boldsymbol{r}}_{mi}]_{\mathcal{M}} + 2\boldsymbol{\omega}_{m/i} \times [\dot{\boldsymbol{r}}_{mi}]_{\mathcal{M}} + [\dot{\boldsymbol{\omega}}_{m/i}]_{\mathcal{M}} \times \boldsymbol{r}_{mi} + \boldsymbol{\omega}_{m/i}\\ \times (\boldsymbol{\omega}_{m/i} \times \boldsymbol{r}_{mi})\end{aligned} \tag{4}$$

where $2\boldsymbol{\omega}_{m/i} \times [\dot{\boldsymbol{r}}_{mi}]_{\mathcal{M}}$ is the *Coriolis acceleration* and $\boldsymbol{\omega}_{m/i} \times (\boldsymbol{\omega}_{m/i} \times \boldsymbol{r}_{mi})$ is the *centripetal acceleration* term.

In the Moon frame we have that $\boldsymbol{r}_{em} = -r_{em}\hat{\boldsymbol{\imath}}_m$, and the spacecraft position vectors with respect to the Moon and to the Earth are defined as follows:

$$\boldsymbol{r}_{mi} = x_i\hat{\boldsymbol{\imath}}_m + y_i\hat{\boldsymbol{\jmath}}_m + z_i\hat{\boldsymbol{k}}_m, \boldsymbol{r}_{ei} = (x_i - r_{em})\hat{\boldsymbol{\imath}}_m + y_i\hat{\boldsymbol{\jmath}}_m + z_i\hat{\boldsymbol{k}}_m$$

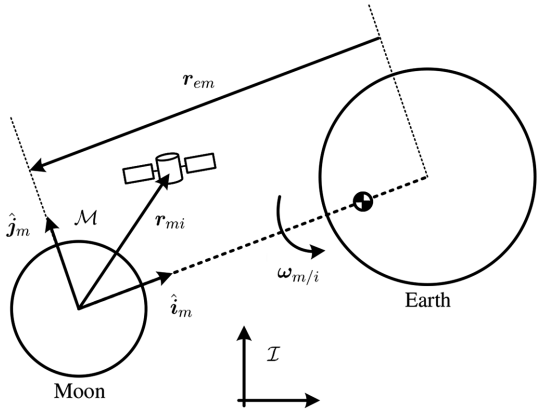

Fig. 1 Moon (synodic) reference frame.

Introducing Eq. (3) in Eq. (4), we obtain the equations of motion for the spacecraft i in the Moon reference frame:

$$[\ddot{\boldsymbol{r}}_{mi}]_{\mathcal{M}} = -2\boldsymbol{\omega}_{m/i}\times[\dot{r}_{mi}]_{\mathcal{M}} - [\dot{\boldsymbol{\omega}}_{m/i}]_{\mathcal{M}}\times\boldsymbol{r}_{mi} - \boldsymbol{\omega}_{m/i}\times(\boldsymbol{\omega}_{m/i}\times\boldsymbol{r}_{mi}) - \mu_m\frac{\boldsymbol{r}_{mi}}{r_{mi}^3} - \mu_e\left(\frac{\boldsymbol{r}_{ei}}{r_{ei}^3} - \frac{\boldsymbol{r}_{em}}{r_{em}^3}\right) \tag{5}$$

or in terms of components in the frame $\mathcal{M}$:

$$\begin{cases} \ddot{x}_i = 2\omega_{m/i}\dot{y}_i + \dot{\omega}_{m/i}y_i + \omega_{m/i}^2 x_i - \mu_m\dfrac{x_i}{r_{mi}^3} - \mu_e\left(\dfrac{x_i - r_{em}}{r_{ei}^3} + \dfrac{1}{r_{em}^2}\right) \\ \ddot{y}_i = -2\omega_{m/i}\dot{x}_i - \dot{\omega}_{m/i}x_i + \omega_{m/i}^2 y_i - \mu_m\dfrac{y_i}{r_{mi}^3} - \mu_e\dfrac{y_i}{r_{ei}^3} \\ \ddot{z}_i = -\mu_m\dfrac{z_i}{r_{mi}^3} - \mu_e\dfrac{z_i}{r_{ei}^3} \end{cases} \tag{6}$$

where the distances of the spacecraft from the Moon and the Earth are given by:

$$r_{ei} = \sqrt{(x_i - r_{em})^2 + y_i^2 + z_i^2}, \qquad r_{mi} = \sqrt{x_i^2 + y_i^2 + z_i^2}$$

Equation (6) can be normalized expressing the distances in units of the Moon orbit semi-major axis a, time in units of the inverse of the Earth–Moon mean angular motion n (i.e., introducing the new time variable $\tau = nt$), and the masses such that $M_e + M_m = 1$. The generic distance x and the associated derivatives are related to the nondimensional variables $\tilde{x}$ as follows:

$$x = a\tilde{x}, \qquad \dot{x} = a\frac{\mathrm{d}\tilde{x}}{\mathrm{d}t} = a\frac{\mathrm{d}\tilde{x}}{\mathrm{d}\tau}\frac{\mathrm{d}\tau}{\mathrm{d}t} = an\tilde{x}', \qquad \ddot{x} = an\frac{\mathrm{d}\tilde{x}'}{\mathrm{d}t} = an^2\tilde{x}''$$

where the prime denotes derivation with respect to the normalized time variable τ. Note that the angular velocity is now expressed in units of n; thus:

$$\omega = n\tilde{\omega}, \qquad \dot{\omega} = \frac{\mathrm{d}\omega}{\mathrm{d}t} = \frac{\mathrm{d}\omega}{\mathrm{d}\tau}\frac{\mathrm{d}\tau}{\mathrm{d}t} = n^2\frac{\mathrm{d}\tilde{\omega}}{\mathrm{d}\tau} = n^2\tilde{\omega}'$$

The *mass ratio* parameter μ is defined as:

$$\mu = \frac{\mu_m}{\mu_e + \mu_m} = \left(1 + \frac{M_e}{M_m}\right)^{-1}$$

Since $M_e + M_m = 1$, Moon and Earth gravitational parameters are then $\mu_m = \mu$ and $\mu_e = 1 - \mu$, respectively.

Equation (6) can now be written in nondimensional form as follows:

$$\begin{cases} \tilde{x}_i'' = 2\tilde{\omega}_{m/i}\tilde{y}_i' + \tilde{\omega}_{m/i}'\tilde{y}_i + \tilde{\omega}_{m/i}^2\tilde{x}_i - \mu\dfrac{\tilde{x}_i}{\tilde{r}_{mi}^3} - (1-\mu)\left(\dfrac{\tilde{x}_i - \tilde{r}_{em}}{\tilde{r}_{ei}^3} + \dfrac{1}{\tilde{r}_{em}^2}\right) \\ \tilde{y}_i'' = 2\tilde{\omega}_{m/i}\tilde{x}_i' - \tilde{\omega}_{m/i}'\tilde{x}_i + \tilde{\omega}_{m/i}^2\tilde{y}_i - \mu\dfrac{\tilde{y}_i}{\tilde{r}_{mi}^3} - (1-\mu)\dfrac{\tilde{y}_i}{\tilde{r}_{ei}^3} \\ \tilde{z}_i'' = -\mu\dfrac{\tilde{z}_i}{\tilde{r}_{mi}^3} - (1-\mu)\dfrac{\tilde{z}_i}{\tilde{r}_{ei}^3} \end{cases} \tag{7}$$

and the normalized distances of the spacecraft from the Earth and the Moon are given by

$$\tilde{r}_{ei} = \sqrt{(\tilde{x}_i - \tilde{r}_{em})^2 + \tilde{y}_i^2 + \tilde{z}_i^2}, \qquad \tilde{r}_{mi} = \sqrt{\tilde{x}_i^2 + \tilde{y}_i^2 + \tilde{z}_i^2}$$

Equation (7) further simplifies if we assume the Moon and the Earth rotating around the Earth–Moon barycenter in circular orbits; that is, we consider the CR3BP. In this case $\tilde{r}_{em} = 1$, $\tilde{\omega}_{m/i} = 1$, and $\tilde{\omega}_{m/i}' = 0$, and Eqs. (7) simplify as follows:

$$\begin{cases} \tilde{x}_i'' = 2\tilde{y}_i' - \tilde{x}_i - \mu\dfrac{\tilde{x}_i}{\tilde{r}_{mi}^3} - (1-\mu)\left(\dfrac{\tilde{x}_i - 1}{\tilde{r}_{ei}^3} + 1\right) \\ \tilde{y}_i'' = -2\tilde{x}_i' + \tilde{y}_i - \mu\dfrac{\tilde{y}_i}{\tilde{r}_{mi}^3} - (1-\mu)\dfrac{\tilde{y}_i}{\tilde{r}_{ei}^3} \\ \tilde{z}_i'' = -\mu\dfrac{\tilde{z}_i}{\tilde{r}_{mi}^3} - (1-\mu)\dfrac{\tilde{z}_i}{\tilde{r}_{ei}^3} \end{cases} \tag{8}$$

with

$$\tilde{r}_{ei} = \sqrt{(\tilde{x}_i - 1)^2 + \tilde{y}_i^2 + \tilde{z}_i^2}, \qquad \tilde{r}_{mi} = \sqrt{\tilde{x}_i^2 + \tilde{y}_i^2 + \tilde{z}_i^2}$$

For the sake of simplicity, in the following sections the overlying tilde will be dropped, and derivation with respect to the normalized time will be denoted with the Newton notation. Thus, all variables and parameters must be considered normalized.

III. Relative Motion Equations in the Restricted Three-Body Problem

A. Exact Relative Dynamics

Consider a *target* and a *chaser* spacecraft orbiting around the Moon and subject to both Earth and Moon gravitational influences. Their equations of motions with respect to the Moon are given by Eq. (3):

$$[\ddot{\boldsymbol{r}}]_{\mathcal{I}} = -\mu\frac{\boldsymbol{r}}{r^3} - (1-\mu)\left(\frac{\boldsymbol{r} + \boldsymbol{r}_{em}}{\|\boldsymbol{r} + \boldsymbol{r}_{em}\|^3} - \frac{\boldsymbol{r}_{em}}{r_{em}^3}\right) \tag{9}$$

$$[\ddot{\boldsymbol{r}}_c]_{\mathcal{I}} = -\mu\frac{\boldsymbol{r}_c}{r_c^3} - (1-\mu)\left(\frac{\boldsymbol{r}_c + \boldsymbol{r}_{em}}{\|\boldsymbol{r}_c + \boldsymbol{r}_{em}\|^3} - \frac{\boldsymbol{r}_{em}}{r_{em}^3}\right) \tag{10}$$

where $\boldsymbol{r}$ and $\boldsymbol{r}_c$ denote target and chaser position with respect to the Moon.

The aim of this section is to describe the motion of the chaser relative to the target in the LVLH frame $\mathcal{L}$: $\{\boldsymbol{r}; \hat{\boldsymbol{\imath}}, \hat{\boldsymbol{\jmath}}, \hat{\boldsymbol{k}}\}$ centered on the target center of mass. The unit vectors of $\mathcal{L}$ are defined as follows:

$$\hat{\boldsymbol{\imath}} = \hat{\boldsymbol{\jmath}}\times\hat{\boldsymbol{k}}, \qquad \hat{\boldsymbol{\jmath}} = -\frac{\boldsymbol{h}}{h}, \qquad \hat{\boldsymbol{k}} = -\frac{\boldsymbol{r}}{r}$$

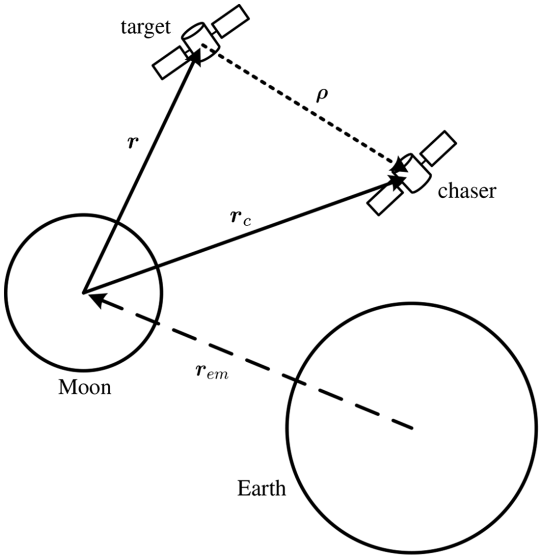

Fig. 2 Target and chaser spacecraft in the three-body system.

where $\boldsymbol{h} = \boldsymbol{r} \times [\dot{\boldsymbol{r}}]_{\mathcal{M}}$ is the target-specific angular momentum with respect to the Moon, and $h = \|\boldsymbol{h}\|$. The unit vectors $\hat{\boldsymbol{\imath}}$, $\hat{\boldsymbol{\jmath}}$, and $\hat{\boldsymbol{k}}$ in the rendezvous literature are generally referred to as *V-bar*, *H-bar*, and *R-bar*, respectively [3]. Note that the LVLH frame is defined with respect to the Moon, because the target is supposed to fly on lunar orbits, and vehicles incoming from the Moon surface or lower and higher orbits are expected to approach the target (as, for instance, is envisaged in the HLEPP [10]).

With reference to Fig. 2, the chaser position with respect to the Moon is given by:

$$\boldsymbol{r}_c = \boldsymbol{r} + \boldsymbol{\rho} \tag{11}$$

where $\boldsymbol{\rho}$ is the relative position of the chaser with respect to the target. The time derivative of Eq. (11) in the inertial frame is:

$$[\dot{\boldsymbol{r}}_c]_{\mathcal{I}} = [\dot{\boldsymbol{r}}]_{\mathcal{I}} + [\dot{\boldsymbol{\rho}}]_{\mathcal{I}} = [\dot{\boldsymbol{r}}]_{\mathcal{I}} + [\dot{\boldsymbol{\rho}}]_{\mathcal{L}} + \boldsymbol{\omega}_{l/i} \times \boldsymbol{\rho} \tag{12}$$

where $\boldsymbol{\omega}_{l/i}$ is the angular velocity of $\mathcal{L}$ (i.e., of the target) with respect to $\mathcal{I}$. Further derivation of Eq. (12) in $\mathcal{I}$ yields:

$$[\ddot{\boldsymbol{r}}_c]_{\mathcal{I}} = [\ddot{\boldsymbol{r}}]_{\mathcal{I}} + [\ddot{\boldsymbol{\rho}}]_{\mathcal{L}} + 2\boldsymbol{\omega}_{l/i} \times [\dot{\boldsymbol{\rho}}]_{\mathcal{L}} + [\dot{\boldsymbol{\omega}}_{l/i}]_{\mathcal{I}} \times \boldsymbol{\rho} + \boldsymbol{\omega}_{l/i} \times (\boldsymbol{\omega}_{l/i} \times \boldsymbol{\rho}) \tag{13}$$

Noting that $[\dot{\boldsymbol{\omega}}_{l/i}]_{\mathcal{I}} = [\dot{\boldsymbol{\omega}}_{l/i}]_{\mathcal{L}}$, and introducing Eqs. (9) and (10) in Eq. (13), we obtain the *nonlinear equations of relative motion* (NERM) in the LVLH frame:

$$\begin{aligned}&[\ddot{\boldsymbol{\rho}}]_{\mathcal{L}} + 2\boldsymbol{\omega}_{l/i} \times [\dot{\boldsymbol{\rho}}]_{\mathcal{L}} + [\dot{\boldsymbol{\omega}}_{l/i}]_{\mathcal{L}} \times \boldsymbol{\rho} + \boldsymbol{\omega}_{l/i} \times (\boldsymbol{\omega}_{l/i} \times \boldsymbol{\rho}) \\ &\quad = \mu\left(\frac{\boldsymbol{r}}{r^3} - \frac{\boldsymbol{r}+\boldsymbol{\rho}}{\|\boldsymbol{r}+\boldsymbol{\rho}\|^3}\right) + (1-\mu)\left(\frac{\boldsymbol{r}+\boldsymbol{r}_{em}}{\|\boldsymbol{r}+\boldsymbol{r}_{em}\|^3} - \frac{\boldsymbol{r}+\boldsymbol{\rho}+\boldsymbol{r}_{em}}{\|\boldsymbol{r}+\boldsymbol{\rho}+\boldsymbol{r}_{em}\|^3}\right)\end{aligned} \tag{14}$$

The angular velocity of the LVLH frame with respect to the inertial frame can be computed by composition of angular velocity vectors:

$$\boldsymbol{\omega}_{l/i} = \boldsymbol{\omega}_{l/m} + \boldsymbol{\omega}_{m/i} \tag{15}$$

where $\boldsymbol{\omega}_{l/m}$ and $\boldsymbol{\omega}_{m/i}$ are the angular velocities of $\mathcal{L}$ with respect to $\mathcal{M}$, and of $\mathcal{M}$ with respect to $\mathcal{I}$, respectively.

The LVLH angular acceleration with respect to $\mathcal{I}$ is given by:

$$[\dot{\boldsymbol{\omega}}_{l/i}]_{\mathcal{L}} = [\dot{\boldsymbol{\omega}}_{l/m}]_{\mathcal{L}} + [\dot{\boldsymbol{\omega}}_{m/i}]_{\mathcal{L}} = [\dot{\boldsymbol{\omega}}_{l/m}]_{\mathcal{L}} + [\dot{\boldsymbol{\omega}}_{m/i}]_{\mathcal{M}} - \boldsymbol{\omega}_{l/m} \times \boldsymbol{\omega}_{m/i} \tag{16}$$

Equation (14), along with Eqs. (15) and (16), composes a set of nonlinear equations with time-varying parameters:

1) $\boldsymbol{r}$, $\boldsymbol{\omega}_{l/m}$, and $[\dot{\boldsymbol{\omega}}_{l/m}]_{\mathcal{L}}$, which depend on the target motion around the Moon

2) $\boldsymbol{r}_{em}$, $\boldsymbol{\omega}_{m/i}$, and $[\dot{\boldsymbol{\omega}}_{m/i}]_{\mathcal{M}}$, characteristics of the Earth–Moon system orbital motion

Equation (14) exactly describes the relative motion in the LVLH frame in the restricted three-body problem, providing that no orbital perturbations act on the spacecraft (e.g., solar radiation pressure). The consideration of the restricted three-body problem provides the option to model the primary bodies in either an elliptic or circular orbit around each other, depending on the three-body system considered.

In the following, the expressions of $\boldsymbol{\omega}_{l/m}$ and $[\dot{\boldsymbol{\omega}}_{l/m}]_{\mathcal{L}}$ are derived, in order to complete the nonlinear description of the relative dynamics in the LVLH frame.

B. LVLH Angular Velocity and Acceleration

We now look for an analytical expression of the LVLH frame angular velocity and acceleration vectors with respect to the Moon frame, which exploits only kinematics relationships. To this end, the same considerations adopted in [21] are here used to find an expression for $\boldsymbol{\omega}_{l/m}$. The angular acceleration $[\dot{\boldsymbol{\omega}}_{l/m}]_{\mathcal{L}}$ is then obtained by differentiation.

Consider the time derivatives of the LVLH frame unit vectors as seen in $\mathcal{M}$:

$$[\dot{\hat{\boldsymbol{\imath}}}]_{\mathcal{M}} = \boldsymbol{\omega}_{l/m} \times \hat{\boldsymbol{\imath}}, \qquad [\dot{\hat{\boldsymbol{\jmath}}}]_{\mathcal{M}} = \boldsymbol{\omega}_{l/m} \times \hat{\boldsymbol{\jmath}}, \qquad [\dot{\hat{\boldsymbol{k}}}]_{\mathcal{M}} = \boldsymbol{\omega}_{l/m} \times \hat{\boldsymbol{k}}$$

Left vector multiplication of the previous expressions by the relative unit vector gives:

$$\begin{aligned}\hat{\boldsymbol{\imath}} \times [\dot{\hat{\boldsymbol{\imath}}}]_{\mathcal{M}} &= \hat{\boldsymbol{\imath}} \times (\boldsymbol{\omega}_{l/m} \times \hat{\boldsymbol{\imath}}) = \boldsymbol{\omega}_{l/m} - (\boldsymbol{\omega}_{l/m} \cdot \hat{\boldsymbol{\imath}})\hat{\boldsymbol{\imath}} \\ \hat{\boldsymbol{\jmath}} \times [\dot{\hat{\boldsymbol{\jmath}}}]_{\mathcal{M}} &= \hat{\boldsymbol{\jmath}} \times (\boldsymbol{\omega}_{l/m} \times \hat{\boldsymbol{\jmath}}) = \boldsymbol{\omega}_{l/m} - (\boldsymbol{\omega}_{l/m} \cdot \hat{\boldsymbol{\jmath}})\hat{\boldsymbol{\jmath}} \\ \hat{\boldsymbol{k}} \times [\dot{\hat{\boldsymbol{k}}}]_{\mathcal{M}} &= \hat{\boldsymbol{k}} \times (\boldsymbol{\omega}_{l/m} \times \hat{\boldsymbol{k}}) = \boldsymbol{\omega}_{l/m} - (\boldsymbol{\omega}_{l/m} \cdot \hat{\boldsymbol{k}})\hat{\boldsymbol{k}}\end{aligned}$$

which can be summed up obtaining:

$$\hat{\boldsymbol{\imath}} \times [\dot{\hat{\boldsymbol{\imath}}}]_{\mathcal{M}} + \hat{\boldsymbol{\jmath}} \times [\dot{\hat{\boldsymbol{\jmath}}}]_{\mathcal{M}} + \hat{\boldsymbol{k}} \times [\dot{\hat{\boldsymbol{k}}}]_{\mathcal{M}} = 2\boldsymbol{\omega}_{l/m} \tag{17}$$

The time derivative of the unit vector $\hat{\boldsymbol{k}}$ is:

$$[\dot{\hat{\boldsymbol{k}}}]_{\mathcal{M}} = -\frac{1}{r}([\dot{\boldsymbol{r}}]_{\mathcal{M}} + \dot{r}\,\hat{\boldsymbol{k}}) \tag{18}$$

Noting that $\boldsymbol{r} = -r\hat{\boldsymbol{k}}$ and $[\dot{\boldsymbol{r}}]_{\mathcal{L}} = -\dot{r}\,\hat{\boldsymbol{k}}$, we can write:

$$\begin{aligned}\dot{r} &= -[\dot{\boldsymbol{r}}]_{\mathcal{L}} \cdot \hat{\boldsymbol{k}} = -[\dot{\boldsymbol{r}}]_{\mathcal{M}} \cdot \hat{\boldsymbol{k}} + (\boldsymbol{\omega}_{l/m} \times \boldsymbol{r}) \cdot \hat{\boldsymbol{k}} = -[\dot{\boldsymbol{r}}]_{\mathcal{M}} \cdot \hat{\boldsymbol{k}} + \boldsymbol{\omega}_{l/m} \cdot (\boldsymbol{r} \times \hat{\boldsymbol{k}}) \\ &= -[\dot{\boldsymbol{r}}]_{\mathcal{M}} \cdot \hat{\boldsymbol{k}}\end{aligned} \tag{19}$$

Substitution of Eq. (19) into Eq. (18) gives:

$$[\dot{\hat{\boldsymbol{k}}}]_{\mathcal{M}} = -\frac{1}{r}(([\dot{\boldsymbol{r}}]_{\mathcal{M}} \cdot \hat{\boldsymbol{\imath}})\hat{\boldsymbol{\imath}} + ([\dot{\boldsymbol{r}}]_{\mathcal{M}} \cdot \hat{\boldsymbol{\jmath}})\hat{\boldsymbol{\jmath}}) = -\frac{1}{r}([\dot{\boldsymbol{r}}]_{\mathcal{M}} \cdot \hat{\boldsymbol{\imath}})\hat{\boldsymbol{\imath}} \tag{20}$$

Note that $[\dot{\boldsymbol{r}}]_{\mathcal{M}} \cdot \hat{\boldsymbol{\jmath}} = 0$ since the target velocity as seen in $\mathcal{M}$ is perpendicular to $\boldsymbol{h}$, by definition of the specific angular momentum.

For the unit vector $\hat{\boldsymbol{\jmath}}$ we have the following time derivative:

$$[\dot{\hat{\boldsymbol{\jmath}}}]_{\mathcal{M}} = -\frac{1}{h^2}(h[\dot{\boldsymbol{h}}]_{\mathcal{M}} - \dot{h}\boldsymbol{h}) \tag{21}$$

According to the definition of $\hat{\boldsymbol{\jmath}}$, we have that $\boldsymbol{h} = -h\hat{\boldsymbol{\jmath}}$. Hence, Eq. (21) simplifies as follows:

$$[\dot{\hat{\boldsymbol{\jmath}}}]_{\mathcal{M}} = -\frac{1}{h}([\dot{\boldsymbol{h}}]_{\mathcal{M}} + \dot{h}\,\hat{\boldsymbol{\jmath}}) \tag{22}$$

Noting that $[\dot{\boldsymbol{h}}]_{\mathcal{L}} = -\dot{h}\,\hat{\boldsymbol{j}}$, we can write $\dot{h}$ as:

$$\dot{h} = -[\dot{\boldsymbol{h}}]_{\mathcal{L}} \cdot \hat{\boldsymbol{j}} = -[\dot{\boldsymbol{h}}]_{\mathcal{M}} \cdot \hat{\boldsymbol{j}} + (\boldsymbol{\omega}_{l/m} \times \boldsymbol{h}) \cdot \hat{\boldsymbol{j}} = -[\dot{\boldsymbol{h}}]_{\mathcal{M}} \cdot \hat{\boldsymbol{j}} \tag{23}$$

since $\boldsymbol{\omega}_{l/m} \times \boldsymbol{h}$ is perpendicular to $\boldsymbol{h}$ and, consequently, to $\hat{\boldsymbol{j}}$. Substitution of Eq. (23) into Eq. (22) yields the time derivative of $\hat{\boldsymbol{j}}$:

$$\begin{aligned}
[\dot{\hat{\boldsymbol{j}}}]_{\mathcal{M}} &= -\frac{1}{h}(([\dot{\boldsymbol{h}}]_{\mathcal{M}} \cdot \hat{\boldsymbol{i}})\hat{\boldsymbol{i}} + ([\dot{\boldsymbol{h}}]_{\mathcal{M}} \cdot \hat{\boldsymbol{k}})\hat{\boldsymbol{k}}) \\
&= -\frac{1}{h}((\boldsymbol{r} \times [\ddot{\boldsymbol{r}}]_{\mathcal{M}}) \cdot \hat{\boldsymbol{i}})\hat{\boldsymbol{i}} \\
&= -\frac{1}{h}([\ddot{\boldsymbol{r}}]_{\mathcal{M}} \cdot (\hat{\boldsymbol{i}} \times \boldsymbol{r}))\hat{\boldsymbol{i}} \\
&= -\frac{r}{h}([\ddot{\boldsymbol{r}}]_{\mathcal{M}} \cdot \hat{\boldsymbol{j}})\hat{\boldsymbol{i}}
\end{aligned} \tag{24}$$

In the previous derivation, the following result was used:

$$[\dot{\boldsymbol{h}}]_{\mathcal{M}} \cdot \hat{\boldsymbol{k}} = (\boldsymbol{r} \times [\ddot{\boldsymbol{r}}]_{\mathcal{M}}) \cdot \hat{\boldsymbol{k}} = 0$$

justified by the fact that $\boldsymbol{r} \times [\ddot{\boldsymbol{r}}]_{\mathcal{M}}$ is perpendicular to $\boldsymbol{r}$, that is, to $\hat{\boldsymbol{k}}$.

The time derivative of $\hat{\boldsymbol{i}}$ is given by:

$$[\dot{\hat{\boldsymbol{i}}}]_{\mathcal{M}} = [\dot{\hat{\boldsymbol{j}}}]_{\mathcal{M}} \times \hat{\boldsymbol{k}} + \hat{\boldsymbol{j}} \times [\dot{\hat{\boldsymbol{k}}}]_{\mathcal{M}} = \frac{r}{h}([\ddot{\boldsymbol{r}}]_{\mathcal{M}} \cdot \hat{\boldsymbol{j}})\hat{\boldsymbol{j}} + \frac{1}{r}([\dot{\boldsymbol{r}}]_{\mathcal{M}} \cdot \hat{\boldsymbol{i}})\hat{\boldsymbol{k}} \tag{25}$$

Substitution of Eqs. (20), (24), and (25) into Eq. (17) yields:

$$\boldsymbol{\omega}_{l/m} = \omega^{y}_{l/m}\hat{\boldsymbol{j}} + \omega^{z}_{l/m}\hat{\boldsymbol{k}} = \left(-\frac{1}{r}[\dot{\boldsymbol{r}}]_{\mathcal{M}} \cdot \hat{\boldsymbol{i}}\right)\hat{\boldsymbol{j}} + \left(\frac{r}{h}[\ddot{\boldsymbol{r}}]_{\mathcal{M}} \cdot \hat{\boldsymbol{j}}\right)\hat{\boldsymbol{k}} \tag{26}$$

Note that in Eq. (26) the component of the angular velocity along the V-bar direction is zero due to the definition of the LVLH frame.

Solution of the dot products in Eq. (26) leads to simplified expressions for $\omega^{y}_{l/m}$ and $\omega^{z}_{l/m}$. For the H-bar component we have:

$$\begin{aligned}
\omega^{y}_{l/m} &= -\frac{1}{r}[\dot{\boldsymbol{r}}]_{\mathcal{M}} \cdot \hat{\boldsymbol{i}} = -\frac{1}{hr^2}[\dot{\boldsymbol{r}}]_{\mathcal{M}} \cdot (\boldsymbol{h} \times \boldsymbol{r}) = -\frac{1}{hr^2}\boldsymbol{h} \cdot (\boldsymbol{r} \times [\dot{\boldsymbol{r}}]_{\mathcal{M}}) \\
&= -\frac{h}{r^2}
\end{aligned} \tag{27}$$

The R-bar component of $\boldsymbol{\omega}_{l/m}$ simplifies as follows:

$$\omega^{z}_{l/m} = \frac{r}{h}[\ddot{\boldsymbol{r}}]_{\mathcal{M}} \cdot \hat{\boldsymbol{j}} = -\frac{r}{h^2}\boldsymbol{h} \cdot [\ddot{\boldsymbol{r}}]_{\mathcal{M}} \tag{28}$$

where the target acceleration is given by Eq. (5):

$$\begin{aligned}
[\ddot{\boldsymbol{r}}]_{\mathcal{M}} = &-2\boldsymbol{\omega}_{m/i} \times [\dot{\boldsymbol{r}}]_{\mathcal{M}} - [\dot{\boldsymbol{\omega}}_{m/i}]_{\mathcal{M}} \times \boldsymbol{r} - \boldsymbol{\omega}_{m/i} \times (\boldsymbol{\omega}_{m/i} \times \boldsymbol{r}) \\
&- \mu\frac{\boldsymbol{r}}{r^3} - (1-\mu)\left(\frac{\boldsymbol{r} + \boldsymbol{r}_{em}}{\|\boldsymbol{r} + \boldsymbol{r}_{em}\|^3} - \frac{\boldsymbol{r}_{em}}{r^3_{em}}\right)
\end{aligned} \tag{29}$$

The components of the angular acceleration in the LVLH frame are obtained by direct derivation of Eqs. (27) and (28).

The angular acceleration along the H-bar is given by:

$$\dot{\omega}^{y}_{l/m} = -\frac{\dot{h}}{r^2} + 2\frac{\dot{r}h}{r^3} = -\frac{1}{r}\left(\frac{\dot{h}}{r} + 2\dot{r}\omega^{y}_{l/m}\right)$$

where the derivative of the norm of $\boldsymbol{r}$ is computed as follows:

$$\dot{r} = \frac{1}{r}\boldsymbol{r} \cdot [\dot{\boldsymbol{r}}]_{\mathcal{M}}$$

The angular acceleration along $\hat{\boldsymbol{k}}$ is:

$$\begin{aligned}
\dot{\omega}^{z}_{l/m} &= -\left(\frac{\dot{r}}{h^2} - 2\frac{r\dot{h}}{h^3}\right)\boldsymbol{h} \cdot [\ddot{\boldsymbol{r}}]_{\mathcal{M}} - \frac{r}{h^2}([\dot{\boldsymbol{h}}]_{\mathcal{M}} \cdot [\ddot{\boldsymbol{r}}]_{\mathcal{M}} + \boldsymbol{h} \cdot [\dddot{\boldsymbol{r}}]_{\mathcal{M}}) \\
&= \left(\frac{\dot{r}}{r} - 2\frac{\dot{h}}{h}\right)\omega^{z}_{l/m} - \frac{r}{h^2}\boldsymbol{h} \cdot [\dddot{\boldsymbol{r}}]_{\mathcal{M}}
\end{aligned}$$

where

$$[\dot{\boldsymbol{h}}]_{\mathcal{M}} \cdot [\ddot{\boldsymbol{r}}]_{\mathcal{M}} = (\boldsymbol{r} \times [\ddot{\boldsymbol{r}}]_{\mathcal{M}}) \cdot [\ddot{\boldsymbol{r}}]_{\mathcal{M}} = 0$$

Given the target acceleration, Eq. (29), the jerk $[\dddot{\boldsymbol{r}}]_{\mathcal{M}}$ can be computed by direct derivation:

$$\begin{aligned}
[\dddot{\boldsymbol{r}}]_{\mathcal{M}} = &-2\boldsymbol{\omega}_{m/i} \times [\ddot{\boldsymbol{r}}]_{\mathcal{M}} - 3[\dot{\boldsymbol{\omega}}_{m/i}]_{\mathcal{M}} \times [\dot{\boldsymbol{r}}]_{\mathcal{M}} - [\ddot{\boldsymbol{\omega}}_{m/i}]_{\mathcal{M}} \\
&\times \boldsymbol{r} - [\dot{\boldsymbol{\omega}}_{m/i}]_{\mathcal{M}} \times (\boldsymbol{\omega}_{m/i} \times \boldsymbol{r}) - \boldsymbol{\omega}_{m/i} \times ([\dot{\boldsymbol{\omega}}_{m/i}]_{\mathcal{M}} \times \boldsymbol{r}) - \boldsymbol{\omega}_{m/i} \\
&\times (\boldsymbol{\omega}_{m/i} \times [\dot{\boldsymbol{r}}]_{\mathcal{M}}) - \mu\frac{\partial}{\partial \boldsymbol{r}}\left[\frac{\boldsymbol{r}}{r^3}\right][\dot{\boldsymbol{r}}]_{\mathcal{M}} - (1-\mu) \\
&\times \left(\frac{\partial}{\partial \boldsymbol{r}}\left[\frac{\boldsymbol{r} + \boldsymbol{r}_{em}}{\|\boldsymbol{r} + \boldsymbol{r}_{em}\|^3}\right]([\dot{\boldsymbol{r}}]_{\mathcal{M}} + [\dot{r}_{em}]_{\mathcal{M}}) - \frac{\partial}{\partial \boldsymbol{r}_{em}}\left[\frac{\boldsymbol{r}_{em}}{r^3_{em}}\right][\dot{r}_{em}]_{\mathcal{M}}\right)
\end{aligned} \tag{30}$$

where

$$[\dot{\boldsymbol{r}}_{em}]_{\mathcal{M}} = [\dot{\boldsymbol{r}}_{em}]_{\mathcal{I}} - \boldsymbol{\omega}_{m/i} \times \boldsymbol{r}_{em}$$

and

$$\frac{\partial}{\partial \boldsymbol{q}}\left[\frac{\boldsymbol{q}}{q^3}\right] = \frac{1}{q^3}\left(\boldsymbol{I} - 3\frac{\boldsymbol{q}\boldsymbol{q}^T}{q^2}\right)$$

with $\boldsymbol{I}$ denoting the identity matrix.

Concluding, the LVLH angular velocity with respect to the Moon is given by:

$$\begin{cases}
\omega^{y}_{l/m} = -\dfrac{h}{r^2} \\
\omega^{z}_{l/m} = -\dfrac{r}{h^2}\boldsymbol{h} \cdot [\ddot{\boldsymbol{r}}]_{\mathcal{M}}
\end{cases} \tag{31}$$

and its angular acceleration is:

$$\begin{cases}
\dot{\omega}^{y}_{l/m} = -\dfrac{1}{r}\left(\dfrac{\dot{h}}{r} + 2\dot{r}\omega^{y}_{l/m}\right) \\
\dot{\omega}^{z}_{l/m} = \left(\dfrac{\dot{r}}{r} - 2\dfrac{\dot{h}}{h}\right)\omega^{z}_{l/m} - \dfrac{r}{h^2}\boldsymbol{h} \cdot [\dddot{\boldsymbol{r}}]_{\mathcal{M}}
\end{cases} \tag{32}$$

where $[\ddot{\boldsymbol{r}}]_{\mathcal{M}}$ is given by Eq. (29), and $[\dddot{\boldsymbol{r}}]_{\mathcal{M}}$ by Eq. (30).

IV. Simplification of the Equations of Relative Motion

Because of the nonlinearity of the gravitational acceleration and the presence of several time-varying parameters, the equations of relative motions derived in Sec. III, namely, Eq. (14), along with angular velocity and acceleration vectors given by Eqs. (31) and (32), may be difficult to use for the development of guidance and navigation systems. Two possible simplifications are here discussed, aimed at linearizing the equation set and at reducing the number of time-varying parameters.

A. CR3BP Assumption

Under the assumption of primaries revolving in circular orbits, the number of time-varying parameters in Eq. (14) reduces. As a matter of fact, in the CR3BP setup we have the following simplifications:

$$\boldsymbol{r}_{em} = -\hat{\boldsymbol{\imath}}_m, [\dot{r}_{em}]_{\mathcal{M}} = \boldsymbol{0}, \quad \boldsymbol{\omega}_{m/i} = \hat{\boldsymbol{k}}_m, [\dot{\boldsymbol{\omega}}_{m/i}]_{\mathcal{M}} = \boldsymbol{0}, \quad [\ddot{\boldsymbol{\omega}}_{m/i}]_{\mathcal{M}} = \boldsymbol{0}$$

The angular velocity and acceleration of the LVLH frame with respect to the inertial frame simplify as follows:

$$\boldsymbol{\omega}_{l/i} = \boldsymbol{\omega}_{l/m} + \hat{\boldsymbol{k}}_m, \qquad [\dot{\boldsymbol{\omega}}_{l/i}]_{\mathcal{L}} = [\dot{\boldsymbol{\omega}}_{l/m}]_{\mathcal{L}} - \boldsymbol{\omega}_{l/m} \times \hat{\boldsymbol{k}}_m$$

In addition, the computation of the target acceleration and jerk in Eqs. (31b) and (32b) becomes:

$$[\ddot{\boldsymbol{r}}]_{\mathcal{M}} = -2\boldsymbol{\omega}_{m/i} \times [\dot{\boldsymbol{r}}]_{\mathcal{M}} - \boldsymbol{\omega}_{m/i} \times (\boldsymbol{\omega}_{m/i} \times \boldsymbol{r}) - \mu \frac{\boldsymbol{r}}{r^3} - (1-\mu)\left(\frac{\boldsymbol{r}+\boldsymbol{r}_{em}}{\|\boldsymbol{r}+\boldsymbol{r}_{em}\|^3} - \boldsymbol{r}_{em}\right) \tag{33}$$

$$[\dddot{\boldsymbol{r}}]_{\mathcal{M}} = -2\boldsymbol{\omega}_{m/i} \times [\ddot{\boldsymbol{r}}]_{\mathcal{M}} - \boldsymbol{\omega}_{m/i} \times (\boldsymbol{\omega}_{m/i} \times [\dot{\boldsymbol{r}}]_{\mathcal{M}}) - \mu \frac{\partial}{\partial \boldsymbol{r}}\left[\frac{\boldsymbol{r}}{r^3}\right][\dot{\boldsymbol{r}}]_{\mathcal{M}} - (1-\mu)\frac{\partial}{\partial \boldsymbol{r}}\left[\frac{\boldsymbol{r}+\boldsymbol{r}_{em}}{\|\boldsymbol{r}+\boldsymbol{r}_{em}\|^3}\right][\dot{\boldsymbol{r}}]_{\mathcal{M}} \tag{34}$$

B. Linearization of the Gravitational Acceleration

Consider the gravitational acceleration on the chaser, due to the two primaries:

$$\boldsymbol{g}_m(\boldsymbol{r}_c) = -\mu \frac{\boldsymbol{r}_c}{r_c^3}, \qquad \boldsymbol{g}_e(\boldsymbol{r}_c + \boldsymbol{r}_{em}) = -(1-\mu)\frac{\boldsymbol{r}_c + \boldsymbol{r}_{em}}{\|\boldsymbol{r}_c + \boldsymbol{r}_{em}\|^3}$$

These terms can be linearized by means of a Taylor expansion to the first order around the target position. For the lunar gravitational acceleration term we have:

$$\boldsymbol{g}_m(\boldsymbol{r}_c) \approx \boldsymbol{g}_m(\boldsymbol{r}) + \left.\frac{\partial \boldsymbol{g}_m(\boldsymbol{q})}{\partial \boldsymbol{q}}\right|_{\boldsymbol{q}=\boldsymbol{r}} (\boldsymbol{r}_c - \boldsymbol{r}) = -\mu\frac{\boldsymbol{r}}{r^3} - \frac{\mu}{r^3}\left(\boldsymbol{I} - 3\frac{\boldsymbol{r}\boldsymbol{r}^T}{r^2}\right)\boldsymbol{\rho}$$

whereas for the Earth gravitational acceleration term:

$$\begin{aligned}\boldsymbol{g}_e(\boldsymbol{r}_c + \boldsymbol{r}_{em}) &\approx \boldsymbol{g}_e(\boldsymbol{r}+\boldsymbol{r}_{em}) + \left.\frac{\partial \boldsymbol{g}_e(\boldsymbol{q})}{\partial \boldsymbol{q}}\right|_{\boldsymbol{q}=\boldsymbol{r}+\boldsymbol{r}_{em}} (\boldsymbol{r}_c - \boldsymbol{r}) \\ &= -(1-\mu)\frac{\boldsymbol{r}+\boldsymbol{r}_{em}}{\|\boldsymbol{r}+\boldsymbol{r}_{em}\|^3} - \frac{1-\mu}{\|\boldsymbol{r}+\boldsymbol{r}_{em}\|^3} \\ &\quad \times \left(\boldsymbol{I} - 3\frac{(\boldsymbol{r}+\boldsymbol{r}_{em})(\boldsymbol{r}+\boldsymbol{r}_{em})^T}{\|\boldsymbol{r}+\boldsymbol{r}_{em}\|^2}\right)\boldsymbol{\rho}\end{aligned}$$

Hence, the right-hand side of Eq. (14) can be approximated as follows:

$$\begin{aligned}&\mu\left(\frac{\boldsymbol{r}}{r^3} - \frac{\boldsymbol{r}_c}{r_c^3}\right) + (1-\mu)\left(\frac{\boldsymbol{r}+\boldsymbol{r}_{em}}{\|\boldsymbol{r}+\boldsymbol{r}_{em}\|^3} - \frac{\boldsymbol{r}_c+\boldsymbol{r}_{em}}{\|\boldsymbol{r}_c+\boldsymbol{r}_{em}\|^3}\right) \\ &\quad \approx -\frac{\mu}{r^3}\left(\boldsymbol{I} - 3\frac{\boldsymbol{r}\boldsymbol{r}^T}{r^2}\right)\boldsymbol{\rho} - \frac{1-\mu}{\|\boldsymbol{r}+\boldsymbol{r}_{em}\|^3}\left(\boldsymbol{I} - 3\frac{(\boldsymbol{r}+\boldsymbol{r}_{em})(\boldsymbol{r}+\boldsymbol{r}_{em})^T}{\|\boldsymbol{r}+\boldsymbol{r}_{em}\|^2}\right)\boldsymbol{\rho}\end{aligned}$$

obtaining a linear expression of the gravitation accelerations, with respect to the relative position vector.

C. Relative Motion Equation Sets

The possible simplifications discussed in the previous section can be used to derive four equation sets, which describe the relative dynamics with different levels of accuracy.

In the following, the *skew symmetric matrices* associated with angular velocity and acceleration vectors $\boldsymbol{\omega}_{l/i}$ and $[\dot{\boldsymbol{\omega}}_{l/i}]_{\mathcal{L}}$, that is:

$$\boldsymbol{\Omega}_{l/i} = \begin{bmatrix} 0 & -\omega^z_{l/i} & \omega^y_{l/i} \\ \omega^z_{l/i} & 0 & -\omega^x_{l/i} \\ -\omega^y_{l/i} & \omega^x_{l/i} & 0 \end{bmatrix} \quad [\dot{\boldsymbol{\Omega}}_{l/i}]_{\mathcal{L}} = \begin{bmatrix} 0 & -\dot{\omega}^z_{l/i} & \dot{\omega}^y_{l/i} \\ \dot{\omega}^z_{l/i} & 0 & -\dot{\omega}^x_{l/i} \\ -\dot{\omega}^y_{l/i} & \dot{\omega}^x_{l/i} & 0 \end{bmatrix}$$

where

$$\boldsymbol{\omega}_{l/i} = \omega^x_{l/i}\hat{\boldsymbol{\imath}} + \omega^y_{l/i}\hat{\boldsymbol{\jmath}} + \omega^z_{l/i}\hat{\boldsymbol{k}}, \qquad [\dot{\boldsymbol{\omega}}_{l/i}]_{\mathcal{L}} = \dot{\omega}^x_{l/i}\hat{\boldsymbol{\imath}} + \dot{\omega}^y_{l/i}\hat{\boldsymbol{\jmath}} + \dot{\omega}^z_{l/i}\hat{\boldsymbol{k}}$$

are introduced to express the equations of motion in a more compact form.

1. ER3BP-Based Equations: ENERM and ELERM

If the ER3BP problem is considered, then the Moon motion is governed by the classical two-body problem equations, with the Earth as primary body. The quantities $\boldsymbol{r}_{em}$, $\boldsymbol{\omega}_{m/i}$, and $[\boldsymbol{\omega}_{m/i}]_{\mathcal{M}}$ can then be obtained accordingly.

With the name of *elliptic nonlinear equations of relative motion* (ENERM) we will refer to the following equation set:

$$[\ddot{\boldsymbol{\rho}}]_{\mathcal{L}} = -2\boldsymbol{\Omega}_{l/i}[\dot{\boldsymbol{\rho}}]_{\mathcal{L}} - ([\dot{\boldsymbol{\Omega}}_{l/i}]_{\mathcal{L}} + \boldsymbol{\Omega}^2_{l/i})\boldsymbol{\rho} + \mu\left(\frac{\boldsymbol{r}}{r^3} - \frac{\boldsymbol{r}+\boldsymbol{\rho}}{\|\boldsymbol{r}+\boldsymbol{\rho}\|^3}\right) + (1-\mu)\left(\frac{\boldsymbol{r}+\boldsymbol{r}_{em}}{\|\boldsymbol{r}+\boldsymbol{r}_{em}\|^3} - \frac{\boldsymbol{r}+\boldsymbol{\rho}+\boldsymbol{r}_{em}}{\|\boldsymbol{r}+\boldsymbol{\rho}+\boldsymbol{r}_{em}\|^3}\right) \tag{35}$$

characterized by the following time-varying parameters that depend on target and on Moon orbital motion:

1) $\boldsymbol{\omega}_{l/i} = \boldsymbol{\omega}_{l/m} + \boldsymbol{\omega}_{m/i}$;
2) $[\dot{\boldsymbol{\omega}}_{l/i}]_{\mathcal{L}} = [\dot{\boldsymbol{\omega}}_{l/m}]_{\mathcal{L}} + [\dot{\boldsymbol{\omega}}_{m/i}]_{\mathcal{M}} - \boldsymbol{\omega}_{l/m} \times \boldsymbol{\omega}_{m/i}$;
3) $\boldsymbol{\omega}_{l/m}$ given by Eq. (31), with $[\ddot{\boldsymbol{r}}]_{\mathcal{M}}$ as in Eq. (29);
4) $[\dot{\boldsymbol{\omega}}_{l/m}]_{\mathcal{L}}$ given by Eq. (32), with $[\dddot{\boldsymbol{r}}]_{\mathcal{M}}$ as in Eq. (30).

If the chaser acceleration is controllable by means of the control vector $\boldsymbol{u}$, then Eq. (35) can be written as a nonlinear system affine in the control:

$$\dot{\boldsymbol{x}} = \boldsymbol{f}(t, \boldsymbol{x}) + \boldsymbol{B}\boldsymbol{u}, \qquad \boldsymbol{x} = \begin{bmatrix} \boldsymbol{\rho} \\ [\dot{\boldsymbol{\rho}}]_{\mathcal{L}} \end{bmatrix}, \qquad \boldsymbol{B} = \begin{bmatrix} \boldsymbol{0}_{3\times 3} \\ \boldsymbol{I}_3 \end{bmatrix}$$

where $\boldsymbol{I}_n$ is the $n \times n$ identity matrix, and $\boldsymbol{0}_{n\times m}$ is the $n \times m$ zero matrix.

The gravitational acceleration can be linearized as discussed in Sec. IV.B, obtaining the *elliptic linear equations of relative motion* (ELERM):

$$\begin{aligned}[\ddot{\boldsymbol{\rho}}]_{\mathcal{L}} = -2\boldsymbol{\Omega}_{l/i}[\dot{\boldsymbol{\rho}}]_{\mathcal{L}} - \Bigg([\dot{\boldsymbol{\Omega}}_{l/i}]_{\mathcal{L}} + \boldsymbol{\Omega}^2_{l/i} + \frac{\mu}{r^3}\left(\boldsymbol{I} - 3\frac{\boldsymbol{r}\boldsymbol{r}^T}{r^2}\right) \\ + \frac{1-\mu}{\|\boldsymbol{r}+\boldsymbol{r}_{em}\|^3}\left(\boldsymbol{I} - 3\frac{(\boldsymbol{r}+\boldsymbol{r}_{em})(\boldsymbol{r}+\boldsymbol{r}_{em})^T}{\|\boldsymbol{r}+\boldsymbol{r}_{em}\|^2}\right)\Bigg)\boldsymbol{\rho}\end{aligned} \tag{36}$$

with angular velocities and accelerations computed as for the ENERM. Assuming the chaser controllable in acceleration, Eq. (36) can be written in state-space form as follows:

$$\dot{\boldsymbol{x}} = \boldsymbol{A}(t)\boldsymbol{x} + \boldsymbol{B}\boldsymbol{u}$$

with

$$\boldsymbol{A}(t) = \begin{bmatrix} \boldsymbol{0}_{3\times 3} & \boldsymbol{I}_3 \\ \boldsymbol{A}_{\dot{\rho}\rho}(t) & -2\boldsymbol{\Omega}_{l/i}(t) \end{bmatrix}$$

$$\begin{aligned}\boldsymbol{A}_{\dot{\rho}\rho} = &-[\dot{\boldsymbol{\Omega}}_{l/i}]_{\mathcal{L}} - \boldsymbol{\Omega}^2_{l/i} - \frac{\mu}{r^3}\left(\boldsymbol{I} - 3\frac{\boldsymbol{r}\boldsymbol{r}^T}{r^2}\right) \\ &- \frac{1-\mu}{\|\boldsymbol{r}+\boldsymbol{r}_{em}\|^3}\left(\boldsymbol{I} - 3\frac{(\boldsymbol{r}+\boldsymbol{r}_{em})(\boldsymbol{r}+\boldsymbol{r}_{em})^T}{\|\boldsymbol{r}+\boldsymbol{r}_{em}\|^2}\right)\end{aligned}$$

where in the last equation dependence on time was omitted for notation compactness.

2. CR3BP-Based Equations: CNERM and CLERM

If the CR3BP is considered, then the computation of the angular velocities simplifies as follows:

1) $\boldsymbol{\omega}_{l/i} = \boldsymbol{\omega}_{l/m} + \boldsymbol{\omega}_{m/i}$ (as for the elliptic case);
2) $[\dot{\boldsymbol{\omega}}_{l/i}]_{\mathcal{L}} = [\dot{\boldsymbol{\omega}}_{l/m}]_{\mathcal{L}} - \boldsymbol{\omega}_{l/m} \times \hat{\boldsymbol{k}}_m$;
3) $\boldsymbol{\omega}_{l/m}$ is given by Eq. (31), but with $[\ddot{\boldsymbol{r}}]_{\mathcal{M}}$ as in Eq. (33) according to the CR3BP;
4) $[\dot{\boldsymbol{\omega}}_{l/m}]_{\mathcal{L}}$ is given by Eq. (32), with the CR3BP simplified jerk $[\dddot{\boldsymbol{r}}]_{\mathcal{M}}$ in Eq. (34).

The set in Eq. (35) with the CR3BP simplifications will be referred to as *circular nonlinear equations of relative motion* (CNERM),

whereas the set in Eq. (36) under the same simplifications as *circular linear equations of relative motion* (CLERM).

V. Equation Sets Comparison

A. Reference Mission Scenario

To assess and compare the accuracy of the derived equation sets, we considered a reference target orbit inspired by the HLEPP study [10,11]. The study considers a human-assisted robotic mission on the lunar surface, where rovers are tele-operated by astronauts on board a station in lunar orbit, the DSG. Access to the station by vehicles incoming from both the Earth and the lunar surface is one of the most critical aspects of the mission. The study of the relative dynamics for this scenario, and the design of maneuvers for rendezvous and docking with the DSG will provide a step forward in the overall mission design.

The candidate family of orbits for the DSG is the Earth–Moon L1 NRHO [10,22,23]. An example of NRHO belonging to the south subfamily is shown in Fig. 3. The orbit was provided by ESA.

In Fig. 3 the region of the orbit suitable for rendezvous, as suggested by [10,11], is highlighted. To identify the rendezvous region, the *mean anomaly* of the NRHO must be introduced:

$$M(t) = 2\pi \frac{t}{T}$$

where, in analogy to the Keplerian orbits, t is the time from the *periselene* passage, and T is the orbit period. For the orbit in Fig. 3, the average period is $T = 6.9867d$. The periselene is defined as the point where the orbit crosses the x–z plane of the Moon frame $\mathcal{M}$ closest to the Moon, whereas the *aposelene* is defined as the point crossing the same plane farthest from the Moon. The analysis of the stable and central manifolds of the orbit as a function of the mean anomaly was used in [10,11] to identify the recommended rendezvous region $M \in [80°, 280°]$. In this region the existence of the central manifolds enables the design of hovering or station keeping trajectories that can be exploited in the waiting for the clearance for the final approach.

B. Simulations Setup

The equation sets defined in Sec. IV.C were tested and compared, in order to assess their accuracy for different initial spacecraft separations.

Spacecraft motion was simulated according to the ER3BP. The reference scenario discussed in Sec. V.A was used as a benchmark, and the presented NRHO orbit was chosen for selecting target initial states with respect to the Moon.

Table 1 MATLAB simulations setup for equations comparison

Solver setup	
MATLAB solver	ode45
Absolute tolerance	1×10^{-20}
Relative tolerance	1×10^{-13}
Maximum step	$T/10^4$
Simulation time t_f	12 h
Earth–Moon system, from [25]	
μ	1.215×10^{-2}
a	384,400 km
n	2.661699×10^{-6} rad/s
e	0.05490

Table 2 Monte Carlo simulation parameters

	Distance test	Speed test
Target initial conditions (ICs)	25 $M(t_0)$, linearly distributed in [0, 360°]	
Relative displacements per IC	30, linearly distributed	
Rel. displacements interval	$\rho(t_0) \in [0.01, 100]$ km	$\boldsymbol{\rho}(t_0) = [1,1,1]^T$ km
	$\dot{\boldsymbol{\rho}}(t_0) = \mathbf{0}$	$\dot{\rho}(t_0) \in [0.01, 100]$ m/s
Simulations per rel. displ.	100	
Probability distribution	Uniform over the displacement interval	
No. of simulations per test	$25 \times 30 \times 100 = 75{,}000$	

The three simplified equation sets previously defined, namely, the ELERM, the CNERM, and the CLERM, were implemented in MATLAB/Simulink 2014b. The ENERM set was not included in the comparison because for the ER3BP it corresponds to the exact description of the relative motion. Two relative motion equation sets based on the two-body problem were also considered, in order to understand their applicability to restricted three-body scenarios:

1) the linear equations of relative motion (LERM) [24]:

$$\begin{cases} \ddot{x} = \dot{f}^2\left(1 - \dfrac{r}{p}\right)x - 2\dot{f}\left(\dfrac{\dot{r}}{r}z - \dot{z}\right) \\ \ddot{y} = -\dfrac{r}{p}\dot{f}^2 y \\ \ddot{z} = 2\dot{f}\left(\dfrac{\dot{r}}{r}x - \dot{x}\right) + \dot{f}^2\left(1 + 2\dfrac{r}{p}\right)z \end{cases}$$

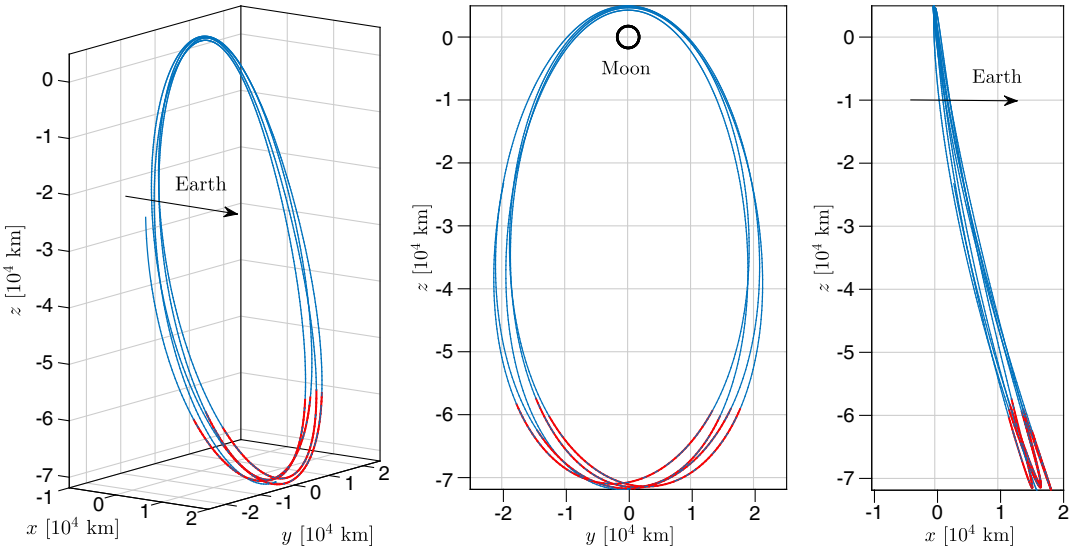

a) Three-dimensional view b) Projection on y-z plane c) Projection on x-z plane

Fig. 3 Reference Earth–Moon L1 south NRHO orbit for target, in the Moon reference frame $\mathcal{M}$. In red the rendezvous zone suggested in [10,11]. Orbit epoch is July 1, 2020.

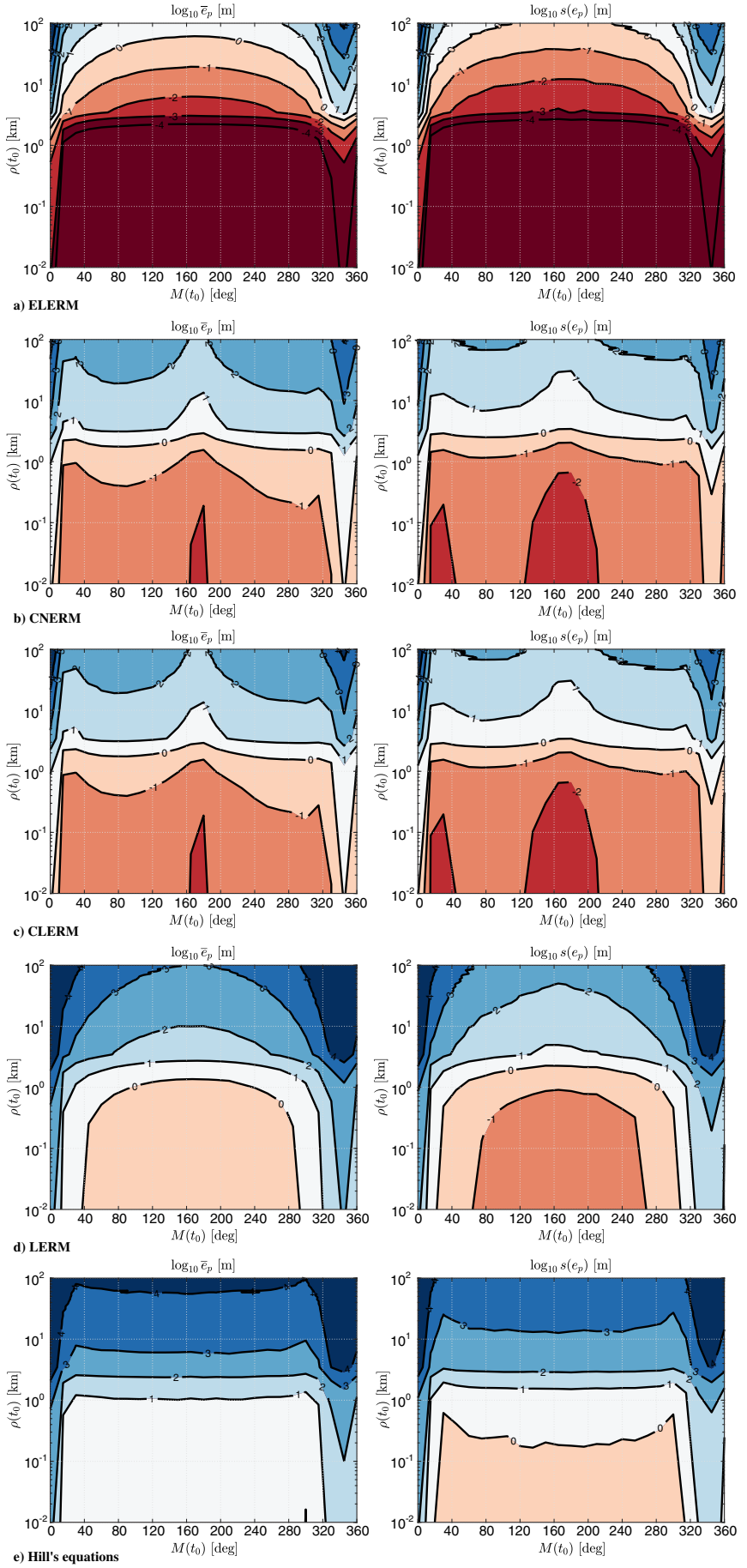

Fig. 4 Distance error e_p for the equation set, distance test: mean $\bar{e}_p$ and standard deviation $s(e_p)$ of the error.

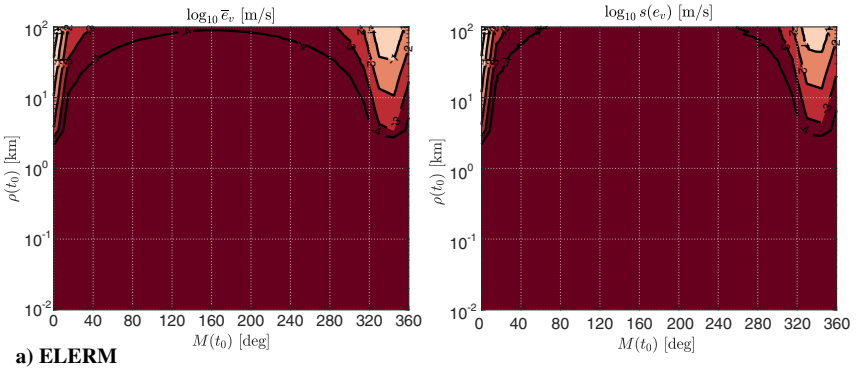

a) ELERM

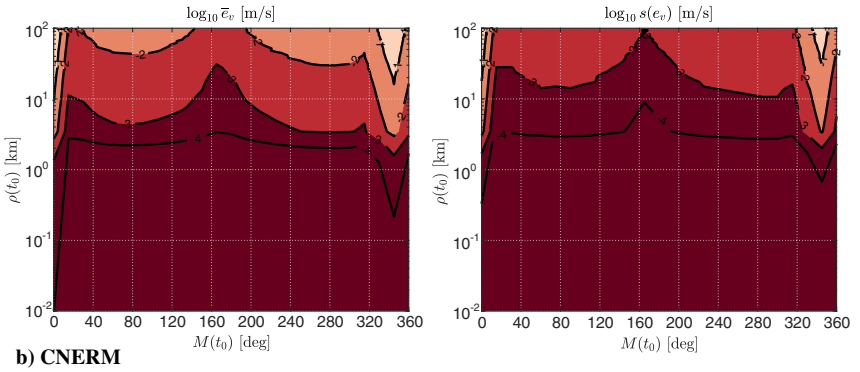

b) CNERM

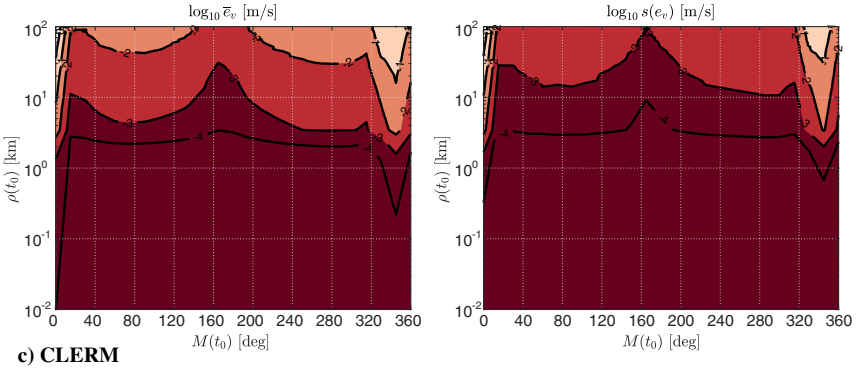

c) CLERM

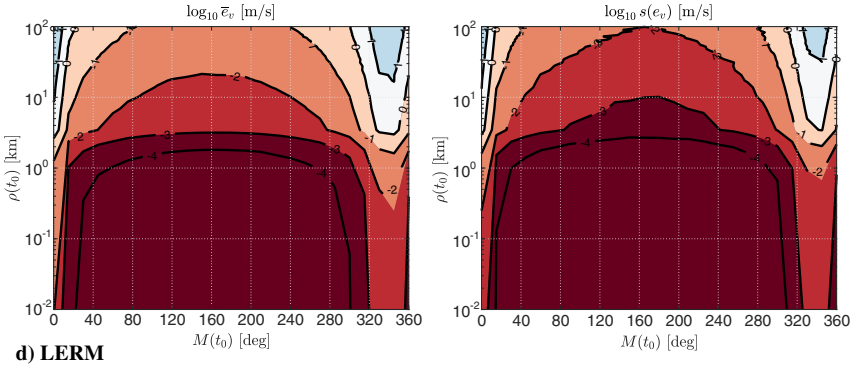

d) LERM

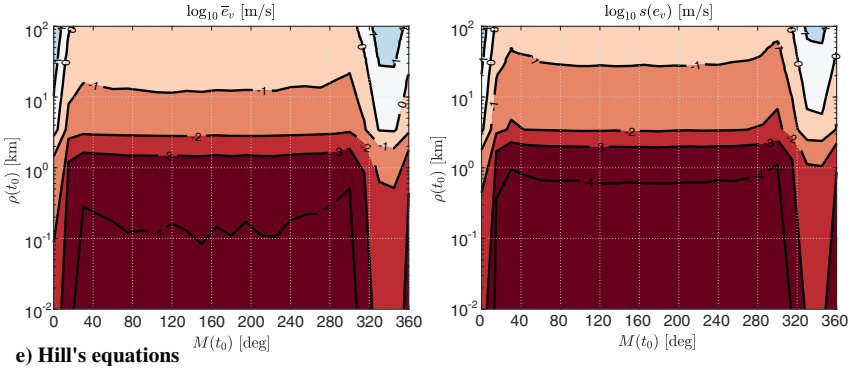

e) Hill's equations

Fig. 5 Speed error e_v for the equation set, distance test: mean $\bar{e}_v$ and standard deviation $s(e_v)$ of the error.

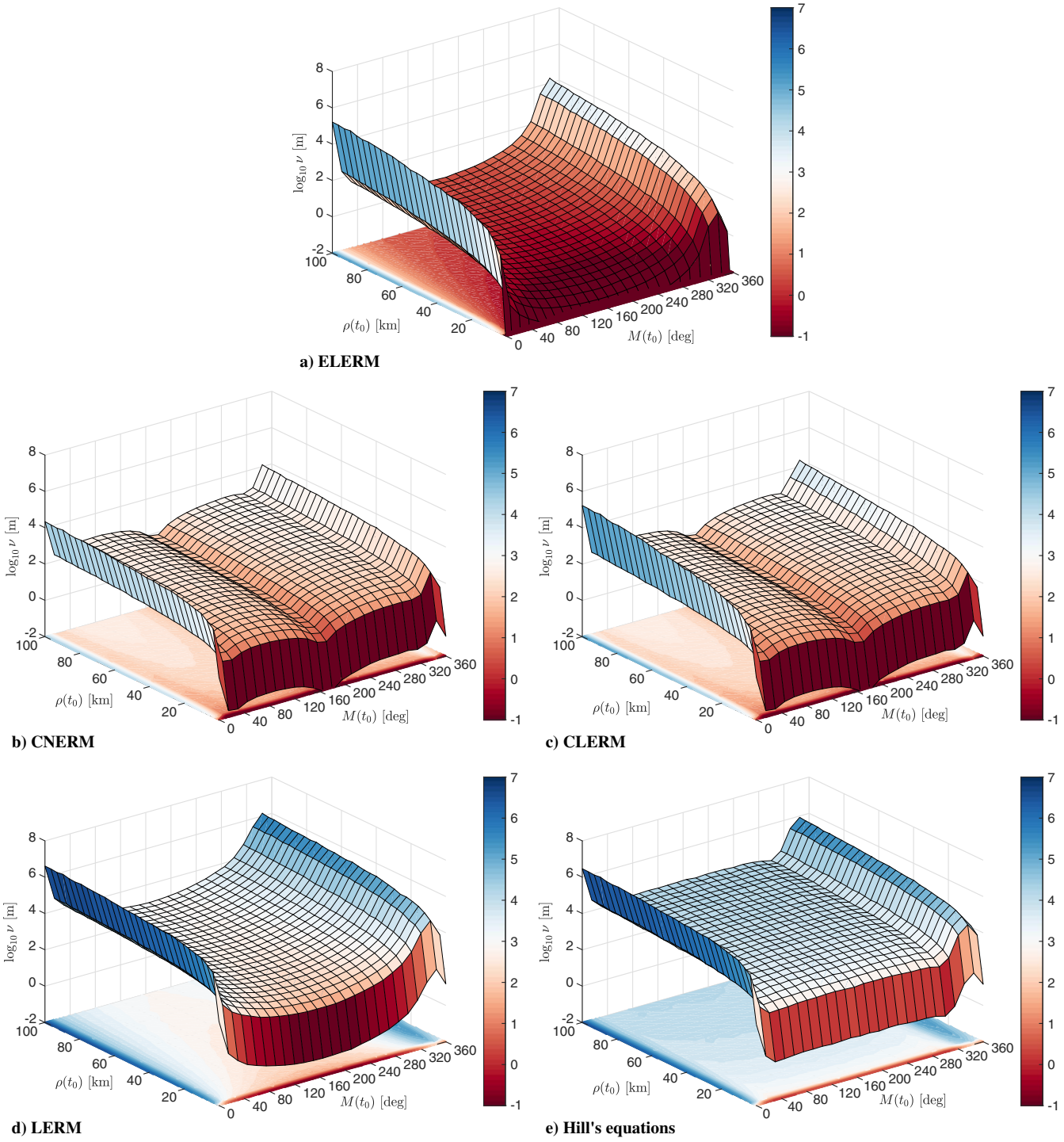

Fig. 6 Error index ν for the equation set, distance test.

where $\boldsymbol{\rho} = x\hat{\boldsymbol{\imath}} + y\hat{\boldsymbol{\jmath}} + z\hat{\boldsymbol{k}}$, p is the target orbit *semilatus rectum*, and $\dot{f}$ denotes the *true anomaly rate*. Both p and $\dot{f}$ were computed from the target initial position and velocity vectors as follows:

$$p = \frac{h(t_0)^2}{\mu}, \qquad \dot{f} = -\frac{h(t_0)}{r^2}, \qquad \text{where } h(t_0) = \|\boldsymbol{r}(t_0) \times [\dot{\boldsymbol{r}}(t_0)]_{\mathcal{M}}\|$$

2) the Hill's or Clohessy–Wiltshire equations [1,3]:

$$\begin{cases} \ddot{x} = 2n\dot{z} \\ \ddot{y} = -n^2 y \\ \ddot{z} = -2n\dot{x} + 3n^2 z \end{cases}$$

where n is the orbit *mean anomaly*, given by $n = 2\pi/T$, with T period of the NRHO orbit.

Two different Monte Carlo simulations were performed to assess the accuracy of the equation sets. The *distance test* analyzes the accuracy as the initial relative separation increases. In particular, for each target initial condition, a given number of relative distances were chosen. For each one, a random initial relative position vector with norm equal to the chosen distance was computed, and the equation sets were propagated. Relative velocity was kept fixed to zero for all the simulations. Conversely, in the *speed test* a set of initial relative speed was chosen, and associated relative velocity vectors were generated randomly. In both tests, target initial conditions were chosen in terms of mean anomaly M along the NRHO orbit. The equation sets were tested over an interval of 12 h. MATLAB solver settings are listed in Table 1. Monte Carlo test parameters are given in Table 2.

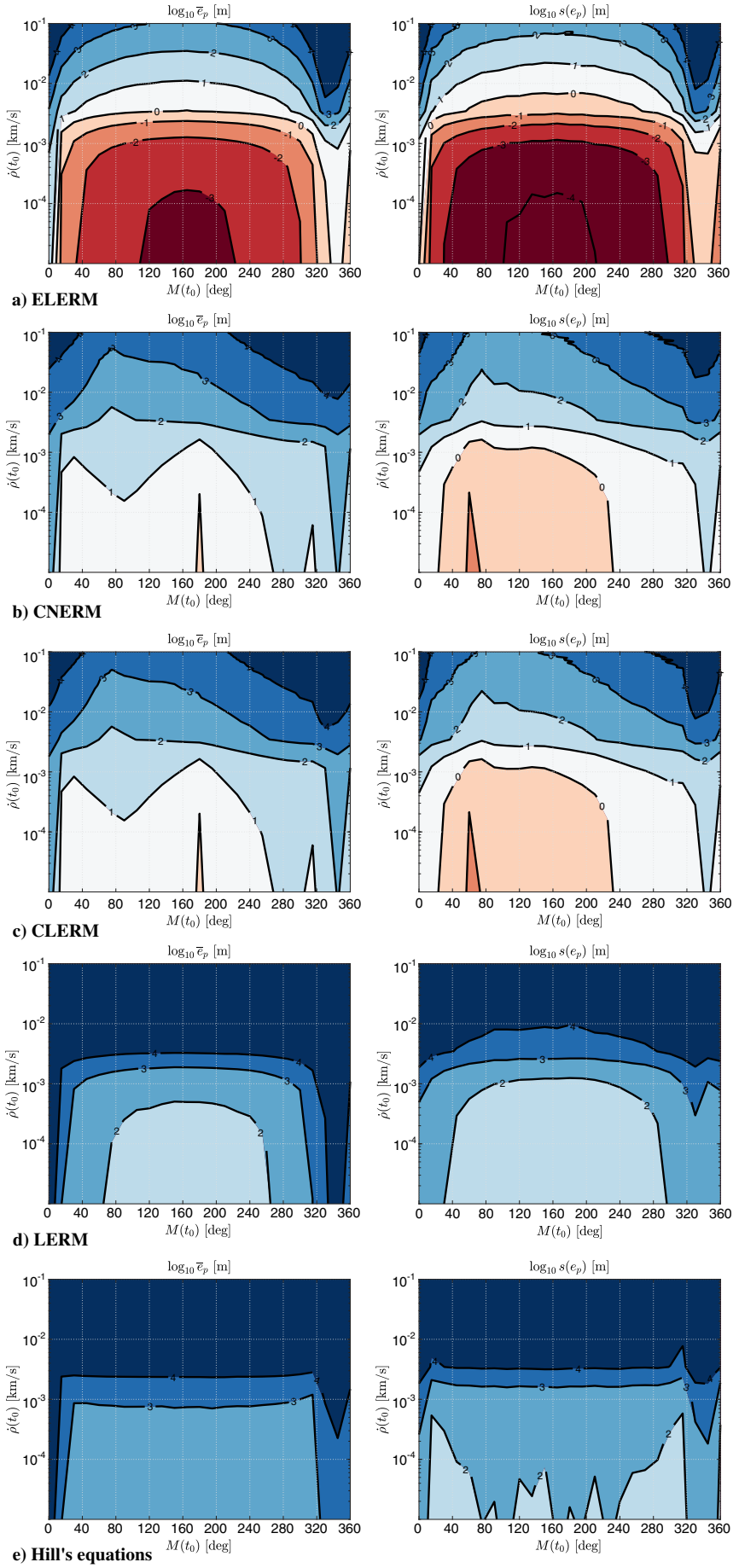

Fig. 7 Distance error e_p for the equation set, speed test: mean $\bar{e}_p$ and standard deviation $s(e_p)$ of the error.

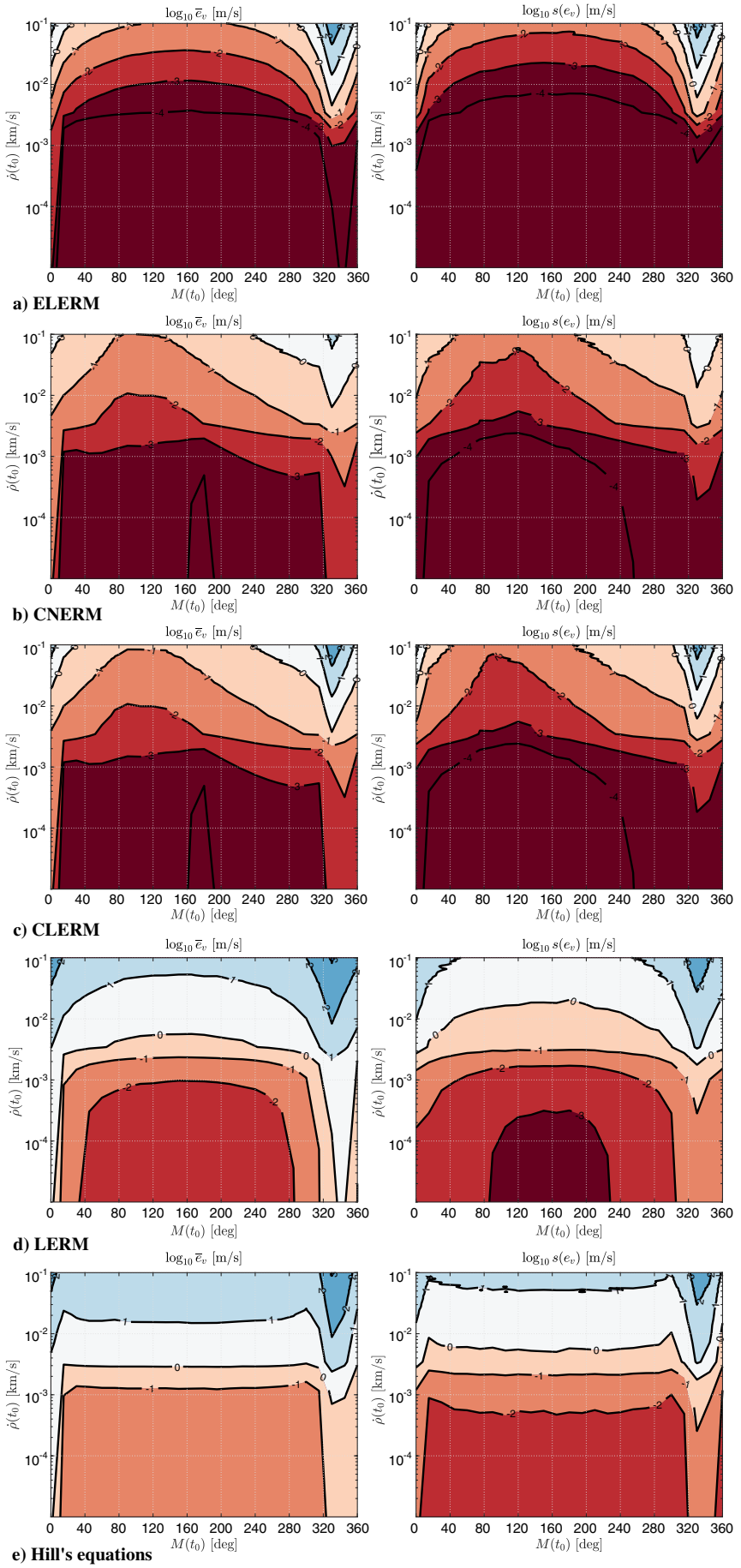

Fig. 8 Speed error e_v for the equation set, speed test: mean $\bar{e}_v$ and standard deviation $s(e_v)$ of the error.

The following performance indexes were defined to compare the equation sets:

1) the maximum distance and speed errors over the simulation interval:

$$e_p = \max_{t\in[t_0,t_f]} \|\boldsymbol{\rho}(t) - \hat{\boldsymbol{\rho}}(t)\|, \qquad e_v = \max_{t\in[t_0,t_f]} \|\dot{\boldsymbol{\rho}}(t) - \dot{\hat{\boldsymbol{\rho}}}(t)\|$$

where the hat denotes the relative position and velocities computed by the tested equation set, whereas the quantities without hat denote the true values.

2) the aggregative performance index:

$$\nu = \max_{t\in[t_0,t_f]} \|\boldsymbol{\xi}(t) - \hat{\boldsymbol{\xi}}(t)\|, \qquad \boldsymbol{\xi} = \begin{bmatrix} \boldsymbol{\rho} \\ n\dot{\boldsymbol{\rho}} \end{bmatrix}$$

where n is the NRHO mean motion. This index, used in [5,26], allows to characterize the overall accuracy of the set. The index ν has dimension of length by adimensionalizing time in the relative velocity using the orbit mean motion.

C. Distance Test Results

The results of the distance test are shown in Figs. 4–6. The ELERM is the most accurate set, with a position error in the order of the meter for almost all the simulated conditions. The CR3BP assumption introduces a significant error, as can be seen comparing the position error of ELERM and CNERM in Fig. 4. In particular, the position error is in the order of the meter only for initial relative distances lower than few kilometers. The linearization of the CNERM does not introduce a great difference in the results, except for target initial conditions near the periselene. This difference can be observed comparing the values of the error index near the mean anomalies $M = 0$ and $M = 360°$ in Figs. 6b and 6c.

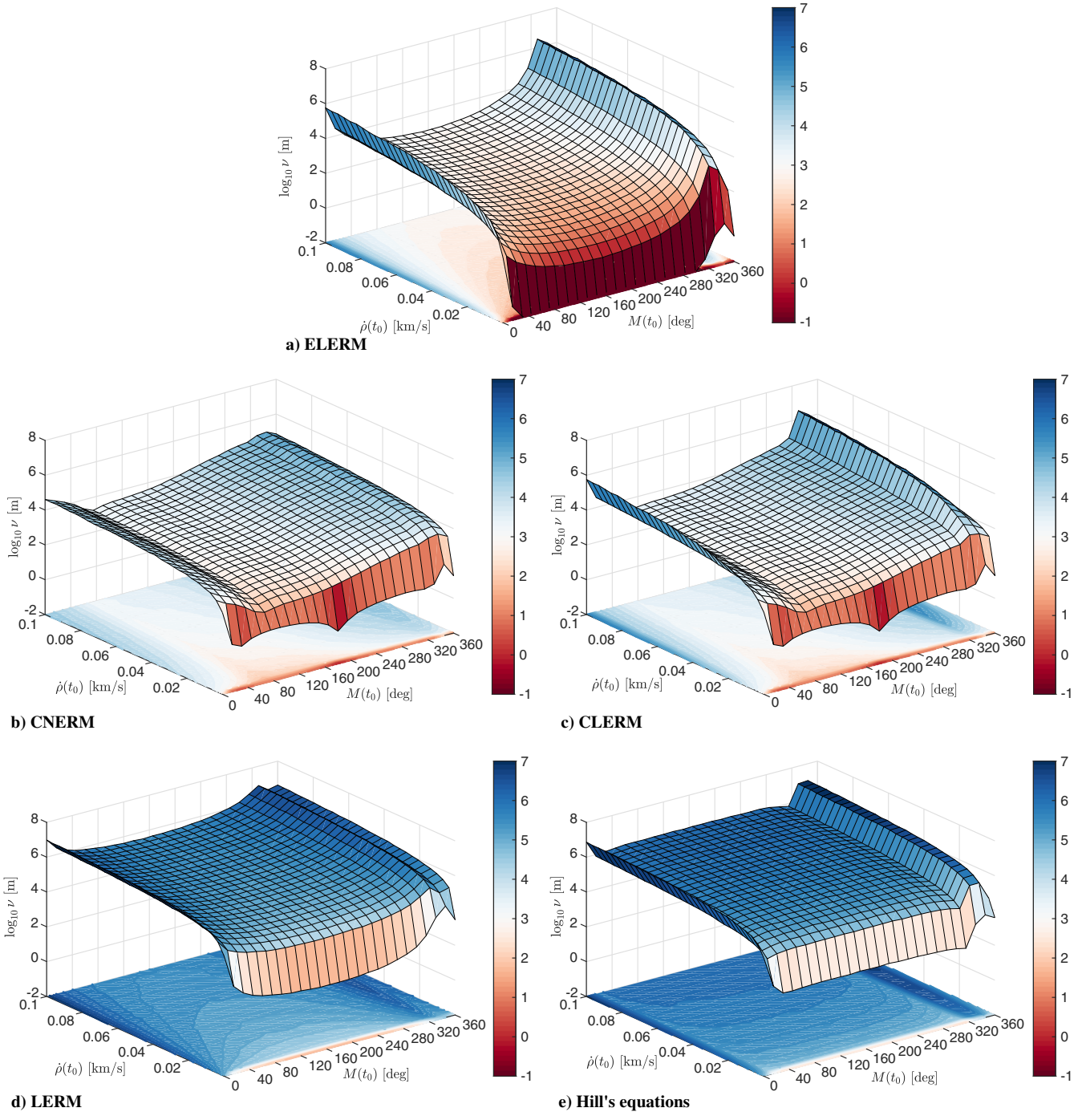

Fig. 9 Error index ν for the equation set, speed test.

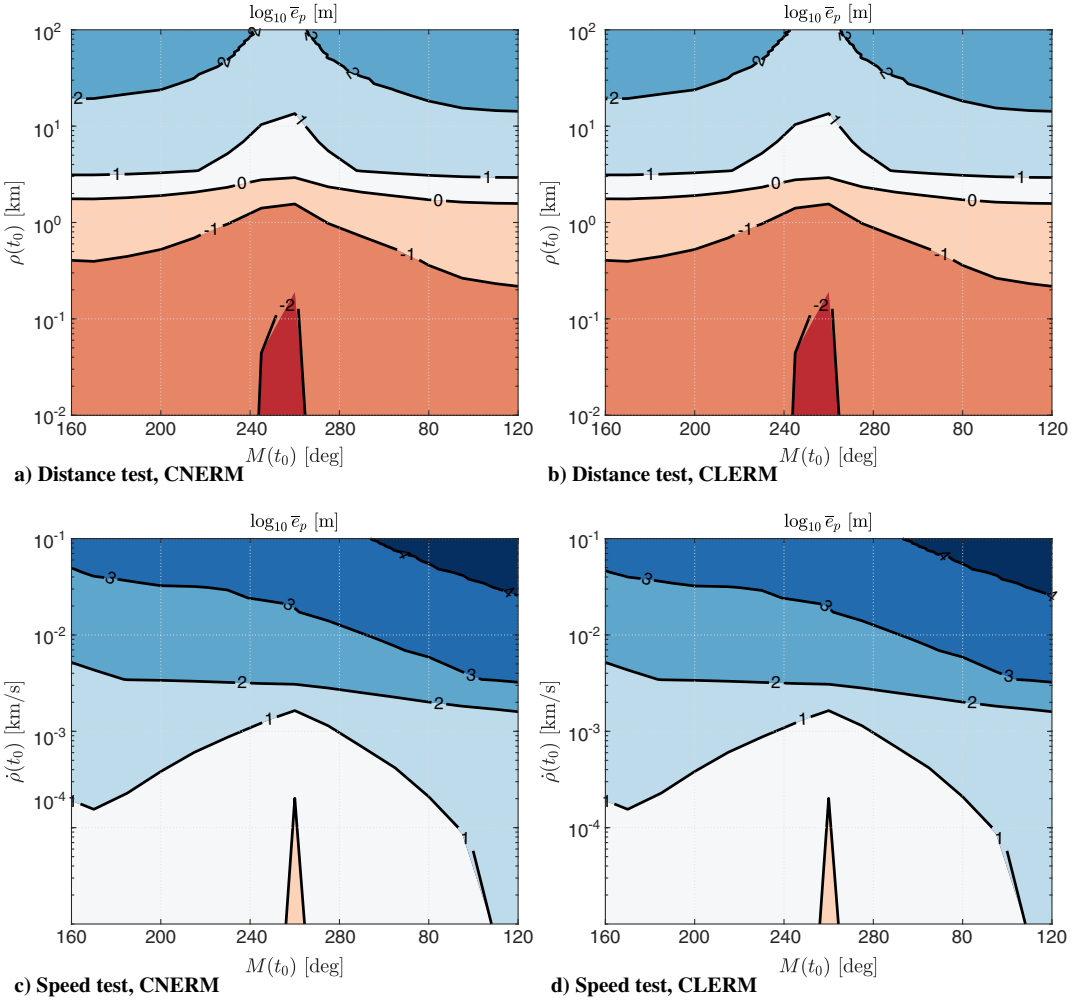

Fig. 10 Average position error $\bar{e}_p$ in the rendezvous zone for the CR3BP-based equation sets.

The two-body-based equations perform worse than the other sets for all the analyzed initial conditions. However, LERM equations show an acceptable error in the order of the meter when the target starts its motion far from the periselene, for initial mean anomalies $M \in [10°, 280°]$.

All the equation sets showed good accuracy in terms of relative velocities, with values of speed errors always below the meter per second, except for large separations in the case of two-body-based equation set (in particular for initial distances above 10 km, with target starting its motion near the periselene).

D. Speed Test Results

The aim of this test is the analysis of the equations accuracy when the initial relative velocity is not zero, as in the distance test. The results are presented in Figs. 7–9.

The ELERM confirmed their higher accuracy compared with the other sets. The CR3BP assumption produces a significant growth in both the position and velocity errors, though in the latter case remain acceptable (below the meter for almost all the tested conditions). Again, there are no significant differences between the CNERM and the CLERM sets.

The two-body-based equation sets showed the worst accuracy, in both position and velocity computation. In particular, for all the test conditions, the position error is above 100 m for the LERM, and above 1 km for the Hill's equations.

The analysis of the error index ν surfaces in Fig. 9 confirms the overall higher accuracy of the ELERM, with respect to the other equation sets.

E. General Remarks

1. *Applicability of CR3BP at the Aposelene*

From the analysis of the position accuracy of the equation sets based on the CR3BP assumption, Figs. 6b, 6c, 7b, and 7c, a region can be found at the aposelene, where the error is small enough to provide a reliable estimation of the chaser relative state. This is highlighted in Fig. 10, where the average position error for the distance and speed tests is evaluated in the rendezvous zone. In the distance test the position error at the aposelene is less than a centimeter for distances below 100 m; see Figs. 10a and 10b. In the speed test, at the aposelene the position error is of the order of the meter for relative speeds below 0.1 m/s. Therefore, CNERM and CLERM equation sets are suitable for relative guidance system design for terminal rendezvous at the aposelene. In particular, CLERM equations are appealing for the design of classical robust controllers due to their linear nature and the reduced number of time-varying parameters, which are the target position with respect to the Moon and the LVLH angular velocity and acceleration vectors. These parameters can be modeled as bounded uncertainties, defined by a prior analysis of their values around the aposelene. Because of the reduced target velocity at the aposelene, the parameters' rate of change will be limited and robust control techniques can be successfully applied.

2. *Linearization Error*

The effects of the linearization are evident near the periselene. Considering, for instance, the distance test, the error index ν at the periselene is larger for the linearized sets ELERM and CLERM than for the nonlinear set CNERM; see Figs. 6a–6c. In Fig. 11 the values of

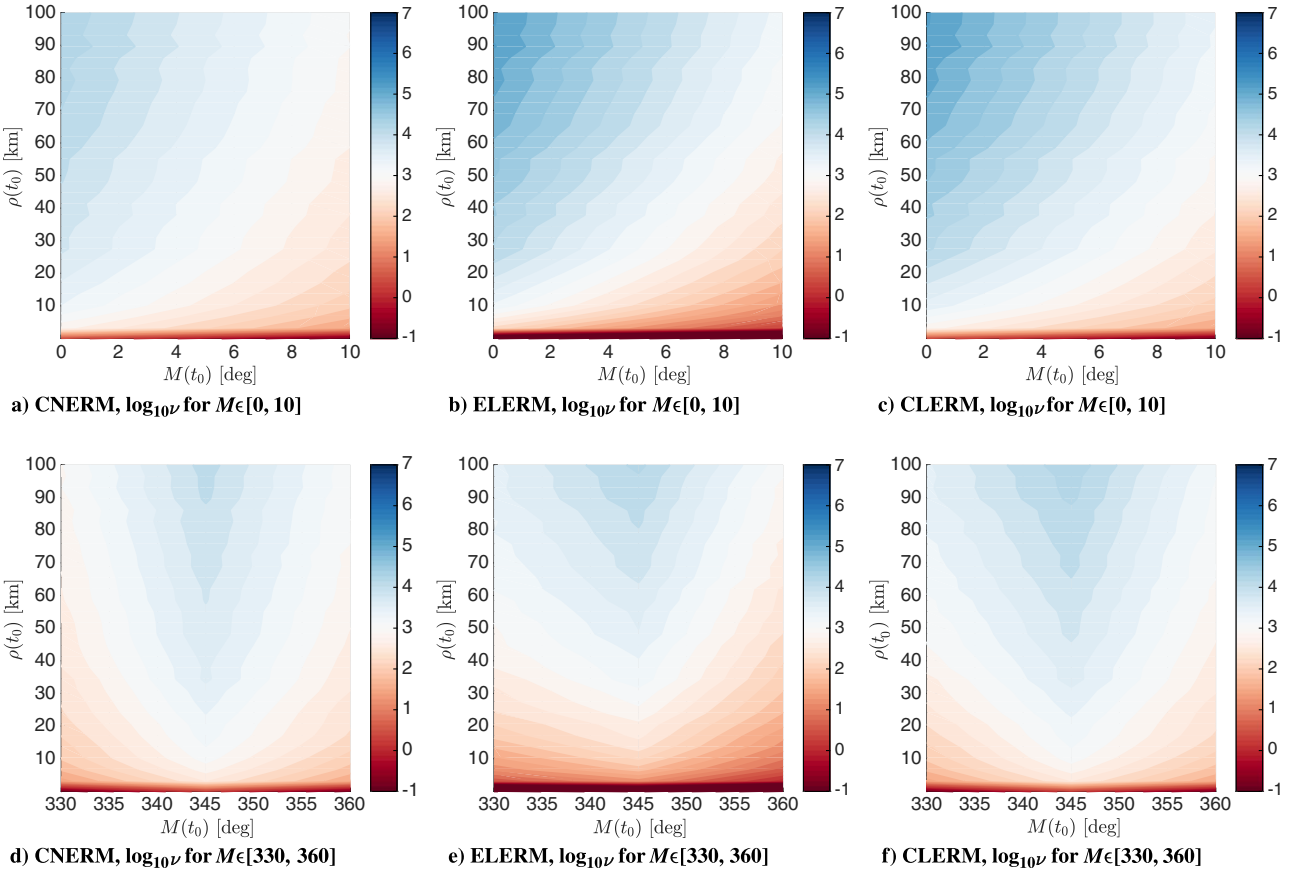

a) CNERM, $\log_{10}\nu$ for $M\epsilon$[0, 10] b) ELERM, $\log_{10}\nu$ for $M\epsilon$[0, 10] c) CLERM, $\log_{10}\nu$ for $M\epsilon$[0, 10]

d) CNERM, $\log_{10}\nu$ for $M\epsilon$[330, 360] e) ELERM, $\log_{10}\nu$ for $M\epsilon$[330, 360] f) CLERM, $\log_{10}\nu$ for $M\epsilon$[330, 360]

Fig. 11 Error index ν for the distance test near the first and the second periselene.

the error index ν for values of the mean anomaly near the first and the second periselene are shown. For distances above 70–80 m the error is clearly larger for the linearized sets, compared with the CNERM equations. For the rest of the target orbit the linearization error is negligible. The cause lies in the high velocity of the target at the periselene that results in a quick separation of the spacecraft, which exceeds the linearization domain of validity.

VI. Conclusions

The relative dynamics in the *local-vertical local-horizon* frame for restricted three-body scenarios were characterized and described by means of a set of nonlinear time-varying equations. Possible simplifications were discussed and applied, obtaining simplified sets with a reduced number of time-varying parameters, and/or linear with respect to the relative motion state. The accuracy of the equation sets was analyzed by means of extensive Monte Carlo simulations, and compared against the two linear equation sets generally employed in Keplerian orbits, namely, linear equations of relative motion and Hill's equations. The tests confirmed that two-body-based equation sets are not suitable for restricted three-body scenarios, especially when the relative velocity becomes significant. The assumption of circular motion for the primaries introduces considerable error, at least for the Earth–Moon system and the orbit chosen as reference target trajectory. However, the error is reduced near the aposelene, making the *circular nonlinear equations of relative motion* and *circular linear equations of relative motion* sets suitable for relative guidance and navigation system design in this regions, provided that robust control techniques are adopted.

Acknowledgments

This work was partially funded by the European Space Agency, under ESA contract No. 4000121575/17/NL/CRS/hh. The views expressed in this paper can in no way be taken to reflect the official opinion of the European Space Agency. The authors would like to thank ESA officer Massimo Casasco for his valuable support.

References

[1] Clohessy, W. H., and Wiltshire, R. S., "Terminal Guidance System for Satellite Rendezvous," *Journal of the Aerospace Sciences*, Vol. 27, No. 9, 1960, pp. 653–658. doi:10.2514/8.8704

[2] Tschauner, J., and Hempel, P., "Rendezvous zu einem in elliptischer Bahn umlaufenden Ziel [Rendez-vous with a target in an elliptical orbit]," *Astronautica Acta*, Vol. 11, No. 2, 1965, pp. 104–109.

[3] Fehse, W., *Automated Rendezvous and Docking of Spacecraft*, Cambridge Univ. Press, Cambridge, U.K., 2003, Chap. 3.

[4] Di Mauro, G., Lawn, M., and Bevilacqua, R., "Survey on Guidance Navigation and Control Requirements for Spacecraft Formation-Flying Missions," *Journal of Guidance, Control, and Dynamics*, Vol. 41, No. 3, 2018, pp. 581–602. doi:10.2514/1.G002868

[5] Sullivan, J., Grimberg, S., and D'Amico, S., "Comprehensive Survey and Assessment of Spacecraft Relative Motion Dynamics Models," *Journal of Guidance, Control, and Dynamics*, Vol. 40, No. 8, 2017, pp. 1837–1859. doi:10.2514/1.G002309

[6] Roscoe, C. W. T., Vadali, S. R., and Alfriend, K. T., "Third-Body Perturbation Effects on Satellite Formations," *The Journal of the Astronautical Sciences*, Vol. 60, No. 3, 2013, pp. 408–433. doi:10.1007/s40295-015-0057-x

[7] Yan, H., Vadali, S. R., and Alfriend, K. T., "State Transition Matrix for Relative Motion Including J2 and Third-Body Perturbations," *Advances in the Astronautical Sciences*, Vol. 152, AAS Paper 14-379, 2014, pp. 2479–2496.

[8] Guffanti, T., D'Amico, S., and Lavagna, M., "Long-Term Analytical Propagation of Satellite Relative Motion in Perturbed Orbits," *Advances in the Astronautical Sciences*, Vol. 160, AAS Paper 17-355, 2017, pp. 2387–2417.

[9] European Space Agency, "Phobos Sample Return—Phobos Moon of Mars Sample Return Mission," CDF Study Rept. CDF-145(A), June 2014, http://sci.esa.int/jump.cfm?oid=55323.

[10] Renk, F., Landgraf, M., and Roedelsperger, M., "Operational Aspects and Low Thrust Transfers for Human-Robotic Exploration Architectures in the Earth-Moon System and Beyond," *Proceedings of 2017 AAS/AIAA Astrodynamics Specialst Conference*, AAS Paper 17-586, Stevenson, WA, Aug. 2017.

[11] Bucci, L., Lavagna, M., and Renk, F., "Relative Dynamics Analysis and Rendezvous Techniques for Lunar Near Rectilinear Halo Orbits," *Proceedings of 68th International Astronautical Congress*, IAC Paper 17-C1.9.12, Adelaide, Australia, Sept. 2017.

[12] Zamaro, M., and Biggs, J. D., "Natural Motion Around the Martian Moon Phobos: The Dynamical Substitutes of the Libration Point Orbits in an Elliptic Three-Body Problem with Gravity Harmonics," *Celestial Mechanics and Dynamical Astronomy*, Vol. 122, No. 3, 2015, pp. 263–302. doi:10.1007/s10569-015-9619-2

[13] Catlin, K. A., and McLaughlin, C. A., "Earth-Moon Triangular Libration Point Spacecraft Formations," *Journal of Spacecraft and Rockets*, Vol. 44, No. 3, 2007, pp. 660–670. doi:10.2514/1.20152

[14] Peng, H., Zhao, J., Wu, Z., and Zhong, W., "Optimal Periodic Controller for Formation Flying on Libration Point Orbits," *Acta Astronautica*, Vol. 69, No. 7, 2011, pp. 537–550. doi:10.1016/j.actaastro.2011.04.020

[15] Ueda, S., Murakami, N., and Ikenaga, T., "A Study on Rendezvous Trajectory Design Utilizing Invariant Manifolds of Cislunar Periodic Orbits," *Proceedings of 2017 AIAA Guidance, Navigation, and Control Conference*, AIAA Paper 2017-1729, Jan. 2017. doi:10.2514/6.2017-1729

[16] Wie, B., *Space Vehicle Dynamics and Control*, 2nd ed., AIAA, Reston, VA, 2008, Chap. 3.

[17] Mand, K., Woffinden, D., Spanos, P., and Zanetti, R., "Rendezvous and Proximity Operations at the Earth-Moon L2 Lagrange Point: Navigation Analysis for Preliminary Trajectory Design," *Advances in the Astronautical Sciences*, Vol. 152, AAS Paper 14-376, 2014, pp. 2425–2444.

[18] Case, S., "Libration Point Orbit Rendezvous Using Linearized Relative Motion Dynamics and Nonlinear Differential Correction," *Advances in the Astronautical Sciences*, Vol. 156, AAS Paper 15-747, 2016, pp. 3599–3612.

[19] Carnà, S. F. R., Bucci, L., and Lavagna, M., "Earth-Moon Multipurpose Orbiting Infrastructure," *Advances in the Astronautical Sciences*, Vol. 158, AAS Paper 16-488, 2016, pp. 1637–1658.

[20] Luquette, R. J., and Sanner, R. M., "Linear State-Space Representation of the Dynamics of Relative Motion, Based on Restricted Three Body Dynamics," *Proceedings of 2004 AIAA Guidance, Navigation, and Control Conference and Exhibit*, AIAA Paper 2004-4783, Aug. 2004. doi:10.2514/6.2004-4783

[21] Casotto, S., "The Equations of Relative Motion in the Orbital Reference Frame," *Celestial Mechanics and Dynamical Astronomy*, Vol. 124, No. 3, 2016, pp. 215–234. doi:10.1007/s10569-015-9660-1

[22] Zimovan, E. M., Howell, K. C., and Davis, D. C., "Near Rectilinear Halo Orbits and Their Application in Cis-Lunar Space," *Proceedings of 3rd IAA Conference on Dynamics and Control of Space Systems*, IAA Paper AAS-DyCoSS3-125, Moscow, May 2017.

[23] Williams, J., Lee, D. E., Whitley, R. J., Bokelmann, K. A., Davis, D. C., and Berry, C. F., "Targeting Cislunar Near Rectilinear Halo Orbits for Human Space Exploration," *Advances in the Astronautical Sciences*, Vol. 160, AAS Paper 17-267, 2017, pp. 3125–3144.

[24] Schaub, H., and Junkins, J. L., *Analytical Mechanics of Space Systems*, 2nd ed., AIAA, Reston, VA, 2009, Chap. 10.

[25] Yoder, C. F., "Astrometric and Geodetic Properties of Earth and the Solar System," *Global Earth Physics: A Handbook of Physical Constants*, edited by T. Ahrens, American Geophysical Union, Washington, D.C., 1995, pp. 1–31. doi:10.1029/RF001p0001

[26] Alfriend, K. T., and Yan, H., "Evaluation and Comparison of Relative Motion Theories," *Journal of Guidance, Control, and Dynamics*, Vol. 28, No. 2, 2005, pp. 254–261. doi:10.2514/1.6691

C. W. Roscoe
Associate Editor